Structural variety of clofaziminium salts

Bodart, Laurie; Tumanov, Nikolay; Wouters, Johan

Published in:
Acta Crystallographica Section B: Structural Science, Crystal Engineering and Materials

DOI:
10.1107/S2052520619007649

Publication date:
2019

Document Version
Peer reviewed version

Structural variety of clofaziminium salts: effect of the counter-ion on clofaziminium conformation and on crystal packing

Authors

Laurie Bodart[a]*, Nikolay Tumanov[a] and Johan Wouters[a]

[a]Chimie, UNamur, Rue de Bruxelles 61, Namur, 5000, Belgium

Correspondence email: laurie.bodart@unamur.be

Funding information Fonds De La Recherche Scientifique - FNRS, research fellow grant.

Crystal packing and conformational comparison of known and new clofaziminium salts.

Abstract Clofazimine (CFZ), is a water-insoluble antimycobacterial agent gaining attention as a multi-drug and extensively-drug resistant tuberculosis treatment. Novel salts of clofazimine are reported with fumaric, succinic, 2,4-dihydroxybenzoic and terephthalic acids as well as with saccharin. The salt structures were obtained by single-crystal X-ray diffraction. Salt with 2,4-dihydroxybenzoic acid and with saccharin are solvated (methanol and acetonitrile respectively). Clofazimine reaction with terephthalic acid led to two cocrystals of salt, one solvated and a non-solvated one. New clofaziminium salts were compared to the currently known ones in terms of crystal packing and clofazimine/ium conformations. Clofaziminium hydrogen succinate presents isostructurality with clofaziminium hydrogen malonate, an already described salt. In structures of clofaziminium terephthalate terephthalic acid cocrystal of salt, solvent evaporation leads to packing and H-bonding modifications. In all structures, clofaziminium conformation is quite well conserved and steric hindrance is observed around the protonated site. Conformational optimization of clofaziminium reveals that this steric hindrance energy penalty is compensated by H-bond interactions with clofaziminium counter-ion.

Keywords: Clofazimine; salt; conformational comparison; crystal packing comparison, counter-ion effect on clofaziminium conformation.

1. Introduction

Clofazimine (CFZ, Figure 1) is an antimycobacterial and anti-inflammatory agent belonging to the family of riminophenazine. First synthesized by Barry *et al.* in 1957, clofazimine has been used worldwide in combination with dapsone and rifampicin as a treatment against leprosy thanks to its bactericidal effect against *M.* leprae (Barry *et al.*, 1957). Besides its anti-leprotic properties, clofazimine is also a drug used to treat multi-drug resistant (MDR) tuberculosis (World Health Organization, 2015). Recently, the apparition of resistant strains of *M. tuberculosis* resulted in a renewal of interest for this drug, since clofazimine exhibit good *in vitro* activity against MDR *Mycobacterium tuberculosis* (Redd *et al.*, 1999; Cholo *et al.*, 2012). However, clofazimine is a very lipophilic molecule resulting in poor solubility and very long half-time (around 70 days in human (Levy, 1974)). This property is associated with undesirable effects such as recrystallization of the compound in the liver and in macrophages (Horstman *et al.*, 2017; Keswani *et al.*, 2015) as well as bioaccumulation resulting in strong side effects, skin discoloration (Job *et al.*, 1990) and poor compliance. Currently, clofazimine has a limited clinical use probably because of its lack of bioavailability and so its limited efficiency. Several methods were investigated to increase clofazimine solubility with various success. Among those were described, for example, clofazimine complexation in cyclodextrins (Salem *et al.*, 2003), preparation of amorphous solid dispersion (Narang & Srivastava, 2002) or clofazimine co-administration with lipid vehicles (O'Reilly *et al.*, 1994).

Because clofazimine is gaining attention as a MDR and extensively drug-resistant *M. tuberculosis* treatment, groups of researchers recently tried new approaches to improve its pharmacological properties. As clofazimine is a weakly basic compound (pKa 9.29 (Keswani *et al.*, 2015)), a possible strategy to increase its solubility is salt formation. In 2012, G. Bolla *et al.* published eight structures of salts, one of these, clofazimine mesylate was 99 time more soluble in 60% EtOH-water media than pure clofazimine (Bolla & Nangia, 2012). In 2016, Bannigan *et al.* investigated clofazimine polymorphism (Bannigan *et al.*, 2016) and more recently they studied the solubility of several clofaziminium salts (Bannigan *et al.*, 2017). Here, we report seven new structures: three salts (clofaziminium hydrogen fumarate, **CFZ-NH$^+$-FA$^-$ (1:1)**, clofaziminium hydrogen succinate, **CFZ-NH$^+$-SA$^-$ (1:1)**) and clofaziminium saccharinate, **CFZ-NH$^+$-SACC$^-$ (1:1)**, two solvated salts (clofaziminium 2,4-dihydroxybenzoate methanol solvate, **CFZ-NH$^+$-2,4DHBA$^-$-MeOH (1:1:1)** and clofaziminium saccharinate acetonitrile solvate, **CFZ-NH$^+$-SACC$^-$-MeCN (1:1:1.4)**), and two cocrystals of salt (structure composed of one cation, one anion and a non-ionized molecule). One is nonstoichiometrically solvated and the other is non-solvated (clofaziminium terephthalate terephthalic acid solvate **CFZ-NH$^+$-TRPTA^{2-}-TRPTA-solvent (1:0.5:0.5:x)** and clofaziminium terephthalate terephthalic acid, **CFZ-NH$^+$-TRPTA^{2-}-TRPTA (1:0.5:0.5)**). Those new salts are compared to the currently known ones in terms of crystal packing and clofaziminium conformation.

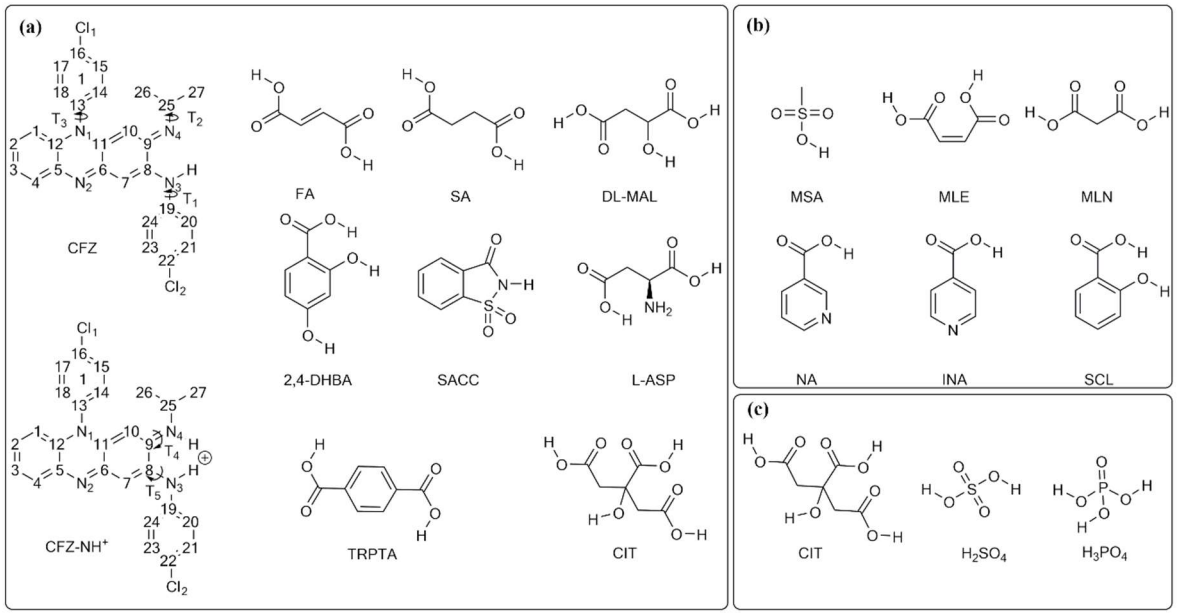

Figure 1 (a) Numbering scheme of clofazimine/ium(CFZ/CFZ-NH^+) (torsions angles: **T1**, C8-N3-C19-C20; **T2**, C9-N4-C25-C27; **T3**, C12-N1-C13-C18 **T4**, H-N4-C9-C8 and **T5**, H-N3-C8-C9) and selected acids in the present work : fumaric acid, succinic acid, DL-malic acid, 2,4-dihydroxybenzoic acid, saccharin, L-aspartic acid, terephthalic acid and citric acid. (b) Acids crystallized with clofazimine by G. Bolla *et al.* (Bolla & Nangia, 2012) and (c) acids crystallized with clofazimine by P. Bannigan *et al.* (Bannigan *et al.*, 2017). CFZ-NH^+-CIT^- (1:1) salt was already described by P. Bannigan *et al.* (Bannigan *et al.*, 2017), in the present study salt formation of CFZ/CIT in 2/1 and 3/1 molar ratios was attempted.

2. Experimental section

2.1. Materials

Clofazimine was purchased from TCI Europe N.V. (Zwindrecht, Belgium), fumaric, 2,4-dihydroxybenzoic and terephthalic acids as well as saccharin were from Sigma-Aldrich (Steinheim, Germany), while succinic acid was purchased from J.T. Baker Chemicals (Deventer, Holland). Crystallization solvents (acetonitrile, methanol, ethyl acetate, and diethyl ether) are commercially available (Acros Organics, Geel, Belgium) and were used without further purification.

2.2. General routes for clofazimine salification.

All samples were prepared by liquid-assisted grinding (LAG) (Frišcic *et al.*, 2009; Shan *et al.*, 2002; Trask *et al.*, 2004; James *et al.*, 2012) with a Retsch MM 400 Mixer Mill apparatus with two grinding jars in which five 2mL Eppendorf tubes can be installed. Each sample grinding was performed with around 100 mg of powder (75mg of clofazimine and corresponding mass of acid to respect 1/1, 2/1 or 3/1 CFZ/acid molar ratios) in presence of 6 to 8 stainless steel grinding balls (2 mm diameter).

Following solvents were used for liquid-assisted ball milling: MeCN for CFZ/FA, CFZ/SA, CFZ/SACC, CFZ/L-ASP, and CFZ/DL-MAL equimolar mixtures as well as for CFZ/CA 2/1 and 3/1 mixtures; MeOH for CFZ/2,4-DHBA 1/1 and EtOAc for CFZ/TRPTA. Powders leading to new diffraction patterns were then involved in crystallization assays by slow evaporation at room temperature in a mixture of MeCN and MeOH, except for CFZ/TRPTA 1/1 powder for which EtOAc was used. For CFZ/DL-MAL crystallization in Et_2O at 4°C as well as in MeCN at room temperature was also attempted.

2.3. Single-crystal X-ray diffraction (SCXRD).

Selected crystals of suitable size were mounted on an Oxford Diffraction Gemini Ultra R system (4-circle kappa platform, Ruby CCD detector). By default Mo radiation was used for data collection, but when the crystal diffracted poorly, Cu radiation was used as it allows enhanced intensities with this Gemini system. In consequence, data were collected using Mo $K\alpha$ (λ = 0.71073 Å) (for **CFZ-NH$^+$-SA$^-$ (1:1)**, **CFZ-NH$^+$-TRPTA^{2-}-TRPTA-solvent (1:0.5:0.5:x)** and **CFZ-NH$^+$-TRPTA^{2-}-TRPTA (1:0.5:0.5)**) or Cu $K\alpha$ (λ = 1.54184 Å) for the other salts (**CFZ-NH$^+$-FA$^-$ (1:1)**, **CFZ-NH$^+$-2,4DHBA$^-$-MeOH (1:1:1)**, **CFZ-NH$^+$-SACC$^-$ (1:1)** and **CFZ-NH$^+$-SACC$^-$-MeCN (1:1:1.4)**). Full data sets were collected either at room temperature (**CFZ-NH$^+$-FA$^-$ (1:1)**, **CFZ-NH$^+$-SA$^-$ (1:1)**, **CFZ-NH$^+$-SACC$^-$ (1:1)**, **CFZ-NH$^+$-2,4DHBA$^-$-MeOH (1:1:1)** and **CFZ-NH$^+$-TRPTA^{2-}-TRPTA (1:0.5:0.5)**) or at 100K (**CFZ-NH$^+$-SACC$^-$-MeCN (1:1:1.4)** and **CFZ-NH$^+$-TRPTA^{2-}-TRPTA-solvent (1:0.5:0.5:x)**). Analytical absorption correction was performed on SCXRD data for structures **CFZ-NH$^+$-FA$^-$ (1:1)**, **CFZ-NH$^+$-SA$^-$ (1:1)**, **CFZ-NH$^+$-TRPTA^{2-}-TRPTA-solvent (1:0.5:0.5:x)** and **CFZ-NH$^+$-TRPTA^{2-}-TRPTA (1:0.5:0.5)** using *CrysAlis PRO* 1.171.38.46 ((Rigaku Oxford Diffraction, 2015)) and 1.171.39.46 ((Rigaku Oxford Diffraction, 2018)). Analytical numeric absorption correction using a multifaceted crystal model based on expressions derived by R.C. Clark & J.S. Reid. (Clark, R. C. & Reid, J. S. (1995). Acta Cryst. A51, 887-897). Empirical absorption correction using spherical harmonics, implemented in SCALE3 ABSPACK scaling algorithm. Gaussian absorption correction was performed on SCXRD data for structures **CFZ-NH$^+$-SACC$^-$-MeCN (1:1:1.4)** and **CFZ-NH$^+$-2,4DHBA$^-$-MeOH (1:1:1)** using *CrysAlis PRO* 1.171.39.46 ((Rigaku Oxford Diffraction, 2018)). Numerical absorption correction based on gaussian integration over a multifaceted crystal model. Empirical absorption correction using spherical harmonics, implemented in SCALE3 ABSPACK scaling algorithm. Multi-scan absorption correction was performed on SCXRD data for structure **CFZ-NH$^+$-SACC$^-$ (1:1)** (*CrysAlis PRO* 1.171.39.46 (Rigaku Oxford Diffraction, 2018) Empirical absorption correction using spherical harmonics, implemented in SCALE3 ABSPACK scaling algorithm.). Structures were solved by dual-space method using SHELXT (Sheldrick, 2015*b*) and then refined by least square method using SHELXL-2018/1 (Sheldrick, 2015*a*) within Olex2 (Dolomanov *et al.*, 2009) and SHELXLE (Hübschle *et al.*, 2011). Non-hydrogen atoms were anisotropically refined. Hydrogen atoms implied in strong hydrogen bonds were localized by Fourier

difference maps while those not implied in H-bonds were refined as riding body by fixing thermal ellipsoids to 1.2 times the one of preceding atom (or 1.5 for methyl group). Several structures are disordered, those structures are: **CFZ-NH$^+$-SA$^-$ (1:1)** (C29 and C30 of hydrogen succinate), **CFZ-NH$^+$-2,4DHBA$^-$-MeOH (1:1:1)** (2,4DHBA$^-$ and MeOH show minor disorder (hydrogen atom of the OH group of disordered MeOH could not be localised by Fourier difference map)), **CFZ-NH$^+$-SACC$^-$ (1:1)** (SACC$^-$ is disordered) and **CFZ-NH$^+$-SACC$^-$-MeCN (1:1:1.4)** (chlorophenyl, 1, on Figure 1 and isopropyl groups of clofazimine as well as acetonitrile, which is disordered over three positions). The structure of cocrystal of salt **CFZ-NH$^+$-TRPTA^{2-}-TRPTA-solvent (1:0.5:0.5:x)** presents solvent accessible voids forming channels but solvent of crystallization could not be unambiguously assigned. Therefore, the original reflection file of **CFZ-NH$^+$-TRPTA^{2-}-TRPTA (1:0.5:0.5)** was submitted to the PLATON SQUEEZE procedure (Spek, 2015). Total potential accessible void volume was determined as 489 Å^3 with an electron count per cell of 141, which corresponds to 2.9 EtOAc molecules in the unit cell. Only low resolution data collection (till 0.9Å) could be performed for the structure **CFZ-NH$^+$-SACC$^-$ (1:1)** because crystals were obtained by desolvating crystals of **CFZ-NH$^+$-SACC$^-$-MeCN (1:1:1.4)** (other methods did not lead to unsolvated crystals).

2.4. Powder X-ray diffraction (PXRD).

Powder diffraction data were collected on an X'PERT PRO PANalytical Bragg-Brentano diffractometer with Cu $K\alpha$ radiation (λ = 1.54184 Å) at 45 kV and 30 mA with a X'Celerator linear detector. Data were collected from 4 to 40° 2θ angles with a step size of 0.0167°. Variable temperature measurement using AntonPaar system were realized at 25°C and then between 30 and 200°C with data collection each 10°C. Calculated powder patterns from SCXRD data were generated with the program Mercury CSD 3.10.2 (Macrae *et al.*, 2008).

2.5. Search in the Cambridge structural database (CSD).

Known structures of clofazimine and clofaziminium salts were retrieved from CSD using ConQuest. In total 15 structures implying clofazimine were retrieved (clofazimine, clofaziminium salts and/or solvates). Three other clofaziminium salts (**CFZ-NH$^+$-CIT$^-$ (1:1)**, **CFZ-NH$^+$-H$_2$PO$_4^-$-H$_2$O (1:1:0.25)** and **CFZ-NH$^+$-HSO$_4^-$-MeOH (1:1:1)**) were available as supplementary data from the publication of Bannigan *et al.)* (Bannigan *et al.*, 2017). All these 18 structures were further analyzed.

2.6. Structure visualization, voids calculation and full interaction maps (FIMs) generation.

Structures were visualized with the CCDC Mercury CSD 3.10.2 software and images were generated using the same program (Macrae *et al.*, 2008). Figures illustrating voids were generated with the display voids option in CCDC Mercury CSD 3.10.2 with a probe radius of 1.2 Å and a grid spacing of 0.1 Å. For the structures of **CFZ-NH$^+$-TRPTA^{2-}-TRPTA-solvent (1:0.5:0.5:x)** and **CFZ-NH$^+$-TRPTA^{2-}-TRPTA (1:0.5:0.5)**, least square planes passing through atoms N1, C5 and C6 of

clofaziminium were calculated with CCDC Mercury CSD 3.10.2 in order to compare crystal packing of the two structures. Full interaction maps were generated within CCDC Mercury CSD 3.10.2. Probes used for FIMs generation were uncharged NH nitrogen, alcohol oxygen, and carbonyl oxygen with a contour level of 6.0. FIMs were generated using coordinates of a clofazimine molecule (from polymorph DAKXUI03) (Figure 2a), a clofaziminium ion (GESHET, **CFZ-NH$^+$-MSA$^-$-H$_2$O (1:1:1)**) (Figures 2b and 6a) and of a clofaziminium ion from **CFZ-NH$^+$-CIT$^-$ (1:1)** (Figure 6b) (for those salts, only clofaziminium was considered for FIMs generation).

2.7. Crystal packing comparison.

Crystal packing comparison and figure of crystal lattice overlay were performed with the crystal packing similarity tool in CCDC Mercury (Macrae *et al.*, 2008) with a packing shell size of 15 molecules and a distance and angle tolerance of 30% and 30° respectively. Molecular differences and structure inversion were allowed while bond types, hydrogen positions, atom's hydrogen count and atom's bond count were ignored. As multi-components systems with different counter-ions were analyzed, the smallest molecular component was ignored for packing overlay. Only **CFZ-NH$^+$-SA$^-$ (1:1)** showed a molecular overlay of 15 molecules out of 15 with **CFZ-NH$^+$-MLN$^-$ (1:1)** (GESGOC).

2.8. Melting point measurement.

Melting points of non-solvated salts were determined visually by using a Büchi Melting point B545 apparatus.

2.9. Clofazimine/clofaziminium overlay.

For each structure of clofazimine/clofaziminium salt (structures of this paper, and these found in the literature) coordinates of one molecule/ion of clofazimine/clofaziminium were selected from asymmetric unit. All selected molecules/ions were overlaid using the Small Molecule overlay tool in Discovery Studio v18 (Dassault Systèmes BIOVIA, 2016). Neither rotatable bonds nor flexible torsions were allowed and the alignment by consensus was performed by a field 50% steric and 50% electrostatic.

2.10. Conformational analysis by quantum mechanics calculations.

Optimization calculations of clofazimine and clofaziminium were performed using density functional theory (DFT) with the m06 functional (Zhao & Truhlar, 2008) and the 6-311G(d) basis set (Frisch *et al.*, 2016). To this aim coordinates of the neutral form of clofazimine was extracted from DAKXUI03 structure while coordinates of the protonated form (clofaziminium) were extracted from **CFZ-NH$^+$-Cl$^-$ (1:1)** (LABQUD) crystal structure.

3. Results and discussion

Acidic compounds to react with clofazimine were selected after full interaction map analysis of clofazimine and clofaziminium. Salification assays were performed by liquid-assisted grinding and powders leading to new diffraction patterns were used in crystallization experiments. In this section, results obtained after salification assays and PXRD measurement are first summarized. Then, new structures are described and compared to the known ones in terms of interaction and crystal packing similarity. Finally, clofazimine and clofaziminium conformations are compared with each other and with the optimized conformations of clofazimine and clofaziminium (in presence or absence of its counter-ion).

3.1. Full interaction maps analysis of CFZ and CFZ-NH$^+$ and choice of acids to react with CFZ.

Full interaction maps (FIMs) were generated to investigate the propensity of clofazimine/clofaziminium to interact with uncharged NH nitrogen, alcohol oxygen, and carbonyl oxygen. FIMs calculations at the 6.0 contour level indicate two main sites of interaction, namely around nitrogen atoms N3 and N4 for the first site and around N2 for the second site (Figure 2). Both sites are common for clofazimine and clofaziminium. However, the interaction between the first site and carbonyl oxygen or OH probes is stronger in the case of clofaziminium (Figure 2 (a) and (b)). From those FIMs analyses, it can be assumed that clofazimine should be able to form salts with several carboxylic acids. Clofaziminium salts with organic acids (methanesulfonic acid, maleic acid, isonicotinic acid, nicotinic acid, salicylic acid and malonic acid) were reported by G. Bolla *et al*. (Bolla & Nangia, 2012) while Bannigan *et al*. obtained clofaziminium salts by reacting clofazimine with organic and inorganic acids (hydrochloric acid, sulphuric acid, nitric acid, oxalic acid, phosphoric acid, citric, formic and acetic acids) (Bannigan *et al.*, 2017). Here, other carboxylic acids (which should protonate N4 of CFZ) were selected to form new clofaziminium salts. 2,4DHBA and DL-MAL were selected because of their alcohol functions which could potentially interact with the N2 site of CFZ. L-ASP was chosen to assess the ability of clofazimine to react with amino-acids (reaction is expected with the carboxylic acid of the side chain). CIT was selected to be reacted in 2/1 and 3/1 CFZ/CIT molar ratios with CFZ to investigate CIT propensity to be unprotonated at multiple sites. Moreover, the potential new structures of CFZ/CIT could be compared to the one obtained by Bannigan *et al*. (Bannigan *et al.*, 2017). FA and SA were chosen for their similarity and so for their potential ability to form isostructural structures. TRPTA was selected to compare CFZ salts obtained with aliphatic *vs* aromatic dicarboxylic acids. Finally, saccharin was chosen to evaluate its propensity to react with clofazimine. Indeed, saccharin has acidic properties despite its lack of carboxylic acid function. Moreover, except terephthalic and 2,4-dihydroxybenzoic acids, the selected compounds are classified either as food additives (Ash & Ash, 2008) or as generally regarded as safe (GRAS) (FDA, 2018).

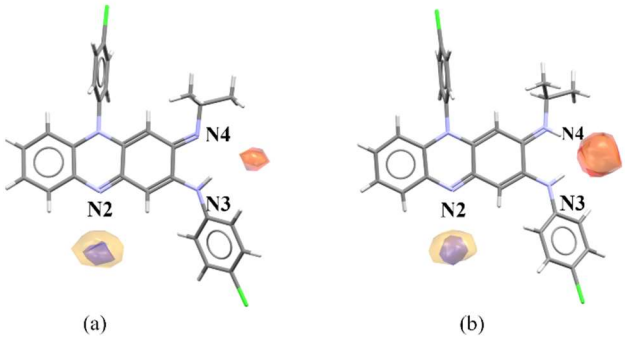

Figure 2 FIMs calculated around clofazimine (a) and clofaziminium (b). Carbonyl oxygen, uncharged NH and alcohol OH probes in red, blue and orange respectively.

3.2. CFZ salification assays and corresponding results.

All liquid-assisted ball milling led to solids with new powder patterns except for CFZ/L-ASP 1/1 (Figure S2). Crystallization assays of all powders except this one were attempted and only, CFZ/DL-MAL did not crystallize in our conditions. Single-crystal X-ray diffraction data were collected on crystals of suitable size. Seven new clofaziminium salt structures were refined. Among those, three are salts (clofaziminium hydrogen fumarate, **CFZ-NH$^+$-FA$^-$ (1:1)**, clofaziminium hydrogen succinate, **CFZ-NH$^+$-SA$^-$ (1:1)** and clofaziminium saccharinate, **CFZ-NH$^+$-SACC$^-$ (1:1)**), two are solvated salts (clofaziminium 2,4-dihydroxybenzoate methanol solvate, **CFZ-NH$^+$-2,4DHBA$^-$-MeOH (1:1:1)** and clofaziminium saccharinate acetonitrile solvate, **CFZ-NH$^+$-SACC$^-$-MeCN (1:1:1.4)**), and two are cocrystals of salt (structure composed of one cation, one anion, and a non-ionized molecule). One is nonstoichiometrically solvated and the other is non-solvated (clofaziminium terephthalate terephthalic acid solvate **CFZ-NH$^+$-TRPTA^{2-}-TRPTA-solvent (1:0.5:0.5:x)** and clofaziminium terephthalate terephthalic acid, **CFZ-NH$^+$-TRPTA^{2-}-TRPTA (1:0.5:0.5)**). The latter was obtained by slowly drying corresponding solvated crystals at room temperature. Crystals of CFZ/CIT 2/1 were obtained. However, the structure is intrinsically disordered and could not be refined even using data collected at 100 K. Its cell parameters and were determined (a: 19.2962 (5), b: 12.3140 (3), c: 23.9105 (6); α: 90, β: 110.667 (3), γ: 90) and Powder pattern of the as synthesized product matches the one calculated from single-crystal data (Figure S2). Finally, CFZ/CIT 3/1 has a powder pattern highly similar to the one obtained after grinding CFZ/CIT 2/1. However, some new peaks are observed (Figure S2). Crystallization assays of CFZ/CIT 3/1 led to crystals of CFZ/CIT 2/1. Results of CFZ salification assays are summarized in Table 1.

Table 1 Clofazimine salification assays and corresponding results.

Acid	pKas (Haynes)	CFZ/Acid ratio	New PXRD?	Crystals?	Structure refined?
FA	3.02; 4.38	1/1	yes	yes	yes
SA	4.21; 5.64	1/1	yes	yes	yes
2,4-DHBA	3.11	1/1	yes	yes	yes
DL-MAL	3.40; 5.11	1/1	yes	no	no
SACC	1.94 (Rowe *et al.*, 2006)	1/1	yes	yes	yes
L-ASP	1.99; 3.90	1/1	no	no	no
TRPTA	3.54; 4.34	1/1	yes	yes	yes
CIT	3.13; 4.76; 6.40	2/1	yes	yes	no*
		3/1	yes	yes**	no

* Structure of **CFZ-NH$^+$- CIT$^-$ (2:1)** is intrinsically disordered. ** Crystallized as **CFZ-NH$^+$- CIT$^-$ (2:1)**.

3.3. Crystal packing description of new CFZ salts.

3.3.1. CFZ-NH$^+$-FA$^-$ (1:1) salt.

Clofaziminium hydrogen fumarate salt (Figure 3 (a)) crystallizes in $P2_1/c$ space group (Table 3). Proton transfer between fumaric acid (O3) and the isopropyl imine of CFZ (N4) occurs. As already observed by P. Bannigan *et al.* (Bannigan *et al.*, 2017), this proton transfer is accompanied by an increase of the iminium angle (angle C9-N4-C25 = 126.02(18)) in comparison with the one of the uncharged clofazimine (C9-N4-C25 around 120° (Table S3)). A $R_2^1(7)$ H-bond motif is observed between FA$^-$ and CFZ-NH$^+$ (N4$^+$-H···O3$^-$ and N3-H···O3$^-$) (Table S2). Hydrogen fumarate forms chains along the *a*-axis through H-bonds ($C_1^1(7)$ motif, O1-H···O3$^-$) (Table S2). A $D(2)$ motif is also present (N3-H···O2) (Table S2). CFZ-NH$^+$ are stacked along *a*-axis in a head-to-tail fashion. PXRD pattern of the as synthesized powder matches the one calculated from single-crystal data (Figure S1). Melting point of **CFZ-NH$^+$-FA$^-$ (1:1)** is 246°C, which is much higher than the starting API (Table 2).

Table 2 Melting points of non-solvated clofaziminium salts.

Compound analyzed	Melting point (°C)
CFZ (DAKXUI01)	219
Fumaric acid	210 * (Temesvári *et al.*, 1971)
Succinic acid	186.9
Saccharin	229.5 (Basavoju *et al.*, 2008)
Terephthalic acid	276 * (Kimyonok & Ulutürk, 2016)
CFZ-NH$^+$-FA$^-$ (1:1)	246
CFZ-NH$^+$-SA$^-$ (1:1)$^-$	214
CFZ-NH$^+$-SACC$^-$ (1:1)	252
CFZ-NH$^+$-TRPTA^{2-}-TRPTA (1:0.5:0.5)	240

* sublimation

3.3.2. CFZ-NH$^+$-SA$^-$ (1:1) salt.

Clofaziminium hydrogen succinate salt (Figure 3 (b)) crystallizes in $P\bar{1}$ space group (Table 3). Proton transfer between succinic acid (O1) and the isopropyl imine of CFZ (N4) occurs, which is confirmed by bond distances reflecting resonance in the carboxylate and by an increase of the iminium angle (Table S3). A $R_2^1(7)$ H-bond motif is observed between SA$^-$ and CFZ-NH$^+$ (N4$^+$-H···O1$^-$ and N3-H···O1$^-$) and an intramolecular H-bond is also present in hydrogen succinate ion ($S_1^1(7)$ motif, O4-H···O2$^-$) (Table S2). 2D sheets are formed through weak C-H···O and C-H···Cl H-bonds (Table S2). PXRD pattern of the as synthesized product matches the one calculated from single-crystal data (Figure S1). This salt melts at 214°C, this melting point is 5°C less than the one of the starting API CFZ (Table 2).

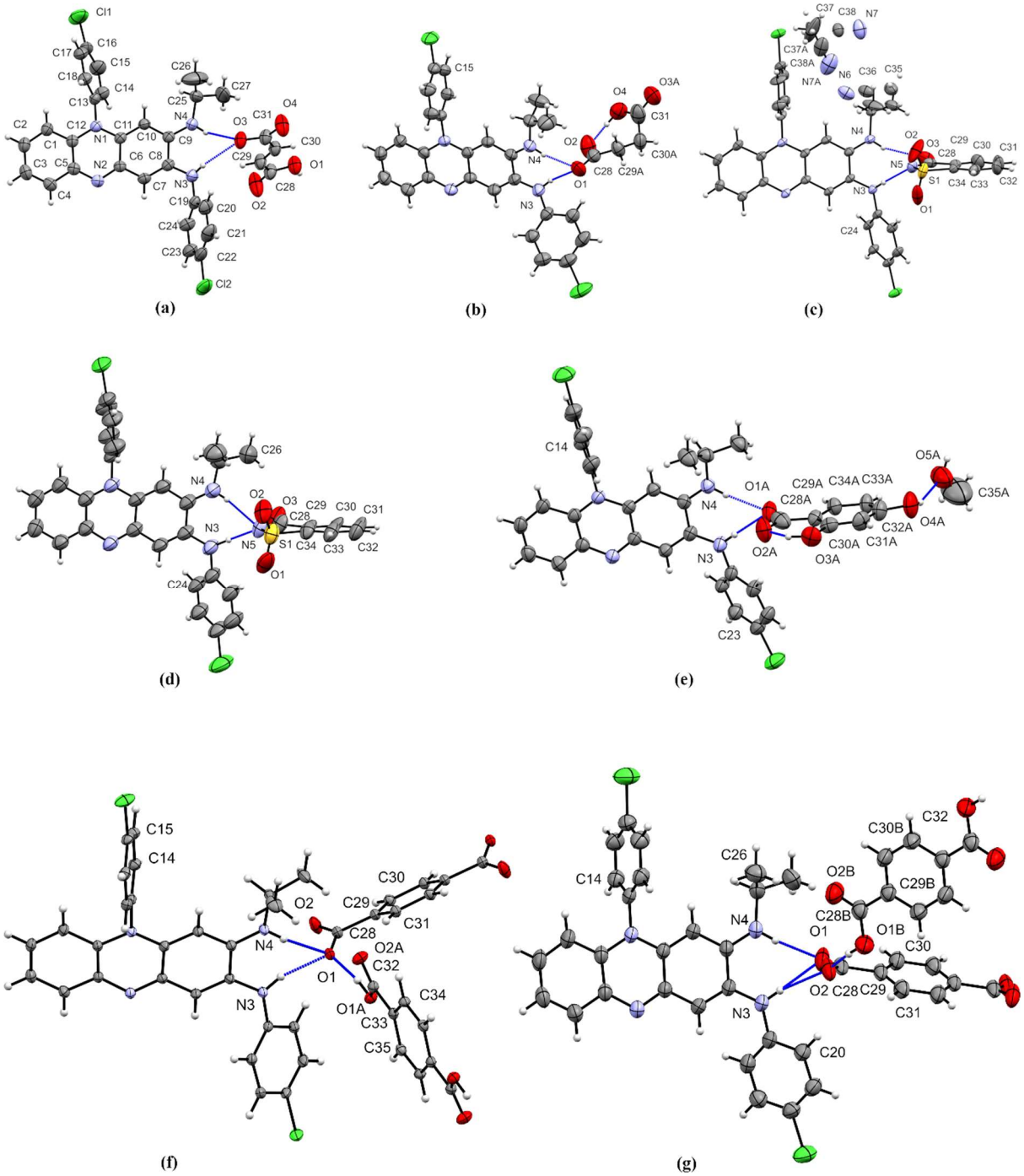

Figure 3 H-bond interactions in the structures of **CFZ-NH$^+$-FA$^-$ (1:1)** (a), **CFZ-NH$^+$-SA$^-$ (1:1)** (b), **CFZ-NH$^+$-SACC$^-$-MeCN (1:1:1.4)** (c), **CFZ-NH$^+$-SACC$^-$ (1:1)** (d) **CFZ-NH$^+$-2,4DHBA$^-$-MeOH (1:1:1)** (e), **CFZ-NH$^+$-TRPTA^{2-}-TRPTA-solvent (1:0.5:0.5:x)** (f) and **CFZ-NH$^+$-TRPTA^{2-}-TRPTA (1:0.5:0.5)** (g). Ellipsoids are drawn at the 50% probability level.

Table 3 Experimental details.

Experiments were carried out using an Xcalibur, Ruby, Gemini Ultra diffractometer. H atoms were treated by a mixture of independent and constrained refinement.

	CFZ-NH$^+$-FA$^-$ (1:1)	**CFZ-NH$^+$-SA$^-$ (1:1)**	**CFZ-NH$^+$-SACC$^-$-MeCN (1:1:1.4)**
Crystal data			
Chemical formula	$C_{27}H_{23}Cl_2N_4^+ \cdot C_4H_3O_4^-$	$C_{27}H_{23}Cl_2N_4^+ \cdot C_4H_5O_4^-$	$C_{27}H_{23}Cl_2N_4^+ \cdot C_7H_4NO_3S^- \cdot 1.393(C_2H_3N)$
M_r	589.46	591.47	713.78
Crystal system, space group	Monoclinic, $P2_1/c$	Triclinic, $P\bar{1}$	Triclinic, $P\bar{1}$
Temperature (K)	295	295	100
a, b, c (Å)	7.47882 (9), 26.0041 (3), 14.78241 (16)	10.6376 (6), 12.2781 (5), 12.7975 (8)	7.9970 (3), 13.5824 (3), 16.6638 (7)
α, β, γ (°)	90, 102.5075 (12), 90	90.079 (4), 113.211 (6), 108.284 (4)	80.214 (3), 80.034 (4), 83.036 (3)
V (Å^3)	2806.65 (6)	1443.57 (15)	1748.87 (11)
Z	4	2	2
Radiation type	Cu $K\alpha$	Mo $K\alpha$	Cu $K\alpha$
μ (mm^{-1})	2.45	0.27	2.61
Crystal size (mm)	0.57 × 0.13 × 0.04	0.57 × 0.42 × 0.03	0.70 × 0.26 × 0.05
Data collection			
Absorption correction	Analytical	Analytical	Gaussian
T_{min}, T_{max}	0.502, 0.915	0.897, 0.990	0.295, 1.000
No. of measured, independent and observed [$I > 2\sigma(I)$] reflections	15078, 4944, 4394	10778, 5090, 3520	17257, 6202, 5378
R_{int}	0.021	0.022	0.033
$(\sin\theta/\lambda)_{max}$ (Å^{-1})	0.597	0.595	0.598
Refinement			
$R[F^2 > 2\sigma(F^2)]$, $wR(F^2)$, S	0.049, 0.136, 1.01	0.045, 0.122, 1.03	0.053, 0.142, 1.05
No. of reflections	4944	5090	6202
No. of parameters	383	412	594
No. of restraints	0	4	137
$\Delta\rho_{max}$, $\Delta\rho_{min}$ (e Å^{-3})	0.46, -0.51	0.24, -0.24	0.61, -0.67

	CFZ-NH$^+$-SACC$^-$ (1:1)	**CFZ-NH$^+$-2,4DHBA$^-$-MeOH (1:1:1)**	**CFZ-NH$^+$-TRPTA^{2-} - TRPTA-solvent (1:0.5:0.5:x)**	**CFZ-NH$^+$-TRPTA^{2-} - TRPTA (1:0.5:0.5)**
Crystal data				
Chemical formula	$C_{27}H_{23}Cl_2N_4^+ \cdot C_7H_4NO_3S^-$	$C_{27}H_{23}Cl_2N_4^+ \cdot C_7H_5O_4^- \cdot CH_4O$	$C_{27}H_{23}Cl_2N_4^+ \cdot 0.5(C_8H_4O_4^{2-}) \cdot 0.5(C_8H_6O_4)$	$C_{27}H_{23}Cl_2N_4^+ \cdot 0.5(C_8H_4O_4^{2-}) \cdot 0.5(C_8H_6O_4)$
M_r	656.56	659.54	639.51	639.51
Crystal system, space group	Triclinic, $P\bar{1}$	Triclinic, $P\bar{1}$	Triclinic, $P\bar{1}$	Triclinic, $P\bar{1}$
Temperature (K)	295	295	100	295
a, b, c (Å)	8.2115 (7), 13.5327 (12), 14.325 (3)	9.4861 (4), 12.5322 (5), 15.3641 (5)	11.7990 (4), 12.0736 (4), 14.6803 (5)	10.4028 (3), 10.8454 (3), 15.4229 (5)
α, β, γ (°)	89.04 (1), 88.864 (10), 83.781 (7)	98.415 (3), 103.379 (3), 110.450 (4)	72.472 (3), 80.688 (3), 72.030 (3)	71.183 (3), 73.984 (3), 76.148 (2)
V (Å^3)	1582.0 (3)	1612.41 (12)	1891.44 (12)	1561.33 (9)
Z	2	2	2	2
Radiation type	Cu $K\alpha$	Cu $K\alpha$	Mo $K\alpha$	Mo $K\alpha$
μ (mm^{-1})	2.82	2.22	0.21	0.25
Crystal size (mm)	0.54 × 0.29 × 0.05	0.49 × 0.12 × 0.06	0.57 × 0.39 × 0.26	0.72 × 0.48 × 0.41
Data collection				
Absorption correction	Multi-scan	Gaussian	Analytical	Analytical
T_{min}, T_{max}	0.549, 1.000	0.539, 0.991	0.917, 0.960	0.886, 0.921
No. of measured, independent and observed [$I > 2\sigma(I)$] reflections	7488, 3783, 2265	15458, 5692, 4965	20823, 11543, 9100	13059, 5704, 4554
R_{int}	0.038	0.021	0.022	0.018
$(\sin\theta/\lambda)_{max}$ (Å^{-1})	0.526	0.597	0.714	0.602
Refinement				
$R[F^2 > 2\sigma(F^2)]$, $wR(F^2)$, S	0.064, 0.190, 1.08	0.037, 0.111, 1.04	0.044, 0.118, 1.03	0.040, 0.109, 1.02
No. of reflections	3783	5692	11543	5704
No. of parameters	525	555	420	420
No. of restraints	483	66	0	0
$\Delta\rho_{max}$, $\Delta\rho_{min}$ (e Å^{-3})	0.23, -0.22	0.24, -0.32	0.41, -0.30	0.23, -0.27

Computer programs: *CrysAlis PRO* 1.171.38.46 (Rigaku OD, 2015), *CrysAlis PRO* 1.171.39.46 (Rigaku OD, 2018), *SHELXT* (Sheldrick, 2015), *SHELXT* 2014/5 (Sheldrick, 2014), *SHELXL2016*/6 (Sheldrick, 2016).

3.3.3. (CFZ-NH$^+$)$_1$(SACC$^-$)$_1$(MeCN)$_{1.4}$ solvated salt.

Clofaziminium saccharinate acetonitrile solvated salt (Figure 3 (c)) crystallizes in $P\bar{1}$ space group (Table 3). Proton transfer between saccharin (N5) and the isopropyl imine of CFZ (N4) occurs and is confirmed by an increase of the iminium angle (Table S3). Acetonitrile solvate is disordered over three positions (first, second and third position occupancies were refined to the following values 0.4640, 0.4890 and 0.440). A $R_2^2(9)$ H-bond motif is observed between SACC$^-$ and CFZ-NH$^+$ (N4$^+$-H···O3 and N3-H···N5$^-$ (Figure 3 (c) and Table S2)). Weak C-H···O H-bonds stabilize head-to-tail stacking of CFZ-NH$^+$ (Table S2).

3.3.4. CFZ-NH$^+$-SACC$^-$ (1:1) salt

Clofaziminium saccharinate (Figure 3 (d)) was obtained by drying crystals of **CFZ-NH$^+$-SACC$^-$-MeCN (1:1:1.4)** at room temperature. The unsolvated salt (**CFZ-NH$^+$-SACC$^-$ (1:1)**) crystallizes in $P\bar{1}$ space group (Table 3). Proton transfer between saccharin (N5) and the isopropyl imine of CFZ (N4) occurs and is confirmed by an increase of the iminium angle (Table S3). A $R_2^1(7)$ H-bond motif is observed between SACC$^-$ and CFZ-NH$^+$ (N4$^+$-H···N5$^-$ and N3-H···N5$^-$ (Figure 3 (c) and Table S2)). Weak C-H···O H-bonds stabilize head-to-tail stacking of CFZ-NH$^+$ (Table S2). It is interesting to notice that liquid-assisted grinding experiment leads to the unsolvated salt. Indeed, the powder pattern of the as synthesized product (CFZ/SACC 1/1 LAG MeCN) matches the one calculated from SCXRD data of **CFZ-NH$^+$-SACC$^-$ (1:1)** and not the one calculated from SCXRD data of **CFZ-NH$^+$-SACC$^-$-MeCN (1:1:1.4)**.

3.3.5. CFZ-NH$^+$-2,4DHBA$^-$-MeOH (1:1:1) solvated salt.

Clofaziminium 2,4-dihydroxybenzoate methanol solvated salt (Figure 3 (e)) crystallizes in $P\bar{1}$ space group (Table 3). Proton transfer between 2,4-dihydroxybenzoic acid (O1) and the isopropyl imine of CFZ (N4) is confirmed by bond distances reflecting resonance in the carboxylate and by an increase of the iminium angle in comparison with the unprotonated form of clofazimine (Table S3). MeOH and 2,4-DHBA$^-$ are slightly disordered. A $R_2^1(7)$ H-bond is observed between 2,4-DHBA$^-$ and CFZ-NH$^+$ (N4$^+$-H···O1A$^-$ and N3-H···O1A$^-$ as well as N4$^+$-H···O1B$^-$ and N3-H···O1B$^-$) (Table S2). An intramolecular H-bond is also present in 2,4-dihydroxybenzoate ($S_1^1(6)$ motif, O3A-H···O2A$^-$ as well as O3B-H···O2B$^-$) (Table S2). Methanol molecules serve as a bridge between two 2,4-DHBA$^-$. Indeed, a $C_2^2(8)$ motif (O4A-H···O5A and O5A-H···O3A) is observed (Table S2) (Figure 4). In the second position of 2,4DHBA$^-$ and MeOH (disordered), the H- bond interactions form between O4B-H···O5B and O5B-H···O4B (Table S2). CFZ-NH$^+$ are stacked in a head-to-tail fashion. This arrangement is further stabilized by weak C-H···O H-bonds (Table S2). Powder pattern of the as synthesized product matches the one calculated from single-crystal data (Figure S1).

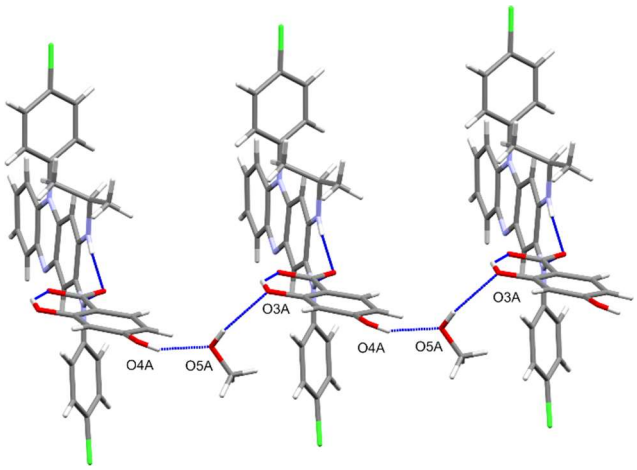

Figure 4 MeOH molecules serve as bridges between 2,4-DHBA$^-$ in the structure of **CFZ-NH$^+$-2,4DHBA$^-$-MeOH (1:1:1)**.

3.3.6. CFZ-NH$^+$-TRPTA^{2-}-TRPTA-solvent (1:0.5:0.5:x) nonstoichiometrically solvated cocrystal of salt.

Clofaziminium terephthalate terephthalic acid nonstoichiometrically solvated cocrystal of salt crystallizes in $P\bar{1}$ space group (Table 3). Its asymmetric unit is composed of one ion of clofaziminium with a half terephthalate ion and a half molecule of terephthalic acid (Figure 3 (f)). Indeed, terephtalic acid and terephthalate are both positioned on an inversion center. Proton transfer between terephthalate (O1) and the isopropyl imine of CFZ (N4) occurs and is confirmed by an increase of the iminium angle (Table S3). Actually, terephthalate anion serves as a linker between two clofaziminium cations, generating three-component CFZ-NH$^+$-TRPTA^{2-}-CFZ-NH$^+$ assemblies (Figure 5 (a)). In those, a $R_2^1(7)$ H-bond motif is observed between TRPTA^{2-} and CFZ-NH$^+$ (N4$^+$-H···O1$^-$ and N3-H···O1$^-$) (Table S2). Those three-component assemblies are interconnected through H-bonds between terephthalate anions and terephthalic acid molecules ($D_1^1(2)$ H-bond motif, O1A-H···O1$^-$) (Figure 5 (a) and Table S2). Weak C-H···O bonds are also present in the structure (Table S2). This arrangement results in solvent accessible voids forming channels (Figure 5 (b) and S4(a)). Although one molecule of ethyl acetate could be localized, high residual electron densities remained in the structure. As all crystallization solvent molecules could not be assigned unambiguously despite low temperature measurement (100K), Platon Squeeze (Spek, 2015) procedure was applied to the data.

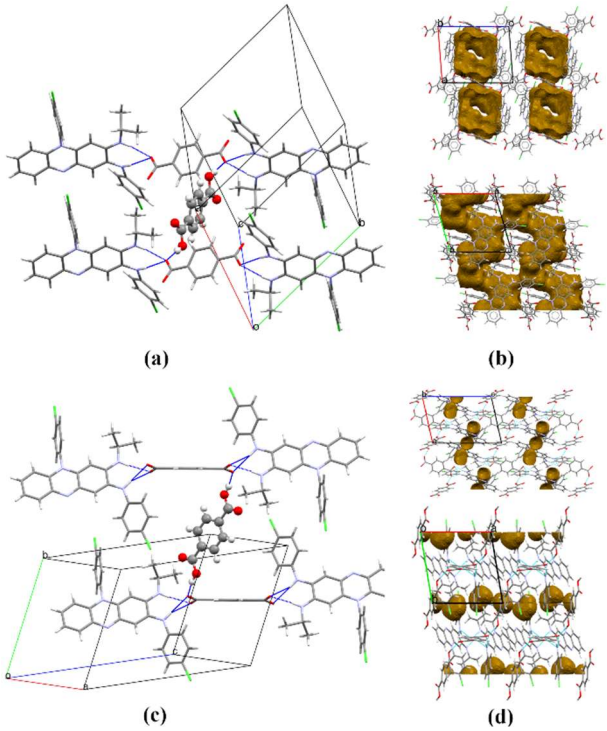

Figure 5 Three-component assemblies (capped stick) linked by terephthalic acid (ball and stick) of **CFZ-NH$^+$-TRPTA^{2-}-TRPTA-solvent (1:0.5:0.5:x)** (a) and of **CFZ-NH$^+$-TRPTA^{2-}-TRPTA (1:0.5:0.5)** (c). Voids along b-axis (top) and c-axis (bottom) of **CFZ-NH$^+$-TRPTA^{2-}-TRPTA-solvent (1:0.5:0.5:x)** (b) and of **CFZ-NH$^+$-TRPTA^{2-}-TRPTA (1:0.5:0.5)** (d).

3.3.7. CFZ-NH$^+$-TRPTA^{2-}-TRPTA (1:0.5:0.5) cocrystal of salt.

Clofaziminium terephthalate terephthalic acid cocrystal of salt (Figure 3 (g)) was obtained by drying **CFZ-NH$^+$-TRPTA^{2-}-TRPTA-solvent (1:0.5:0.5:x)** at room temperature. **CFZ-NH$^+$-TRPTA^{2-}-TRPTA (1:0.5:0.5)** cocrystal of salt crystallizes in $P\bar{1}$ space group (Table 3). Its asymmetric unit is composed of one ion of clofaziminium with a half terephthalate ion and a half molecule of terephthalic acid (Figure 3 (f)). Indeed, terephtalic acid and terephthalate are both positioned on an inversion center. Proton transfer between terephthalate (O1) and the isopropyl imine of CFZ (N4) occurs and is confirmed by an increase of the iminium angle (Table S3). Like in the solvated structure, terephthalate anion serves as a linker between two clofaziminium cations, leading to three-component assemblies. Bifurcated H-bonds between TRPTA^{2-} and CFZ-NH$^+$ are observed ($R_2^2(9)$ motif, N4-H$^+$···O1$^-$ and N3-H···O2$^-$) in addition to the $R_2^1(7)$, N4$^+$-H···O1$^-$ and N3-H···O1$^-$ (Table S2). Three-component assemblies are interconnected through H-bonds with terephthalic acid molecules ($D_1^1(2)$ H-bond motif, O1B-H···O2$^-$) (Figure 5 (c)) (Table S2). Voids are present in the structure of **CFZ-NH$^+$-TRPTA^{2-}-TRPTA (1:0.5:0.5)**, however, they are not interconnected and no channel is observed (Figure 5 (d) and S4(b)). Interestingly, as shown by variable temperature powder X-ray diffraction, this non-solvated structure can be obtained by heating the batch powder synthesized by LAG with EtOAc as solvent (Figure S3).

3.4. CFZ-counter ion interaction comparison.

Full interaction map analyses revealed two possible sites of interaction around clofazimine, namely, near nitrogen atoms N3 and N4 for the first site and around N2 for the second one. Analysis of the 18 known structures (15 on CSD and 3 supplied as supplementary data from the article of Bannigan et al. (Bannigan *et al.*, 2017)) and the seven new ones described in this paper reveals that first site is implied in all salt structures while the second one is only implied in two structures. One structure is the hydrated salt **CFZ-NH$^+$-MSA$^-$-H$_2$O (1:1:1)**. Indeed, N2 interacts through H-bonds with a water molecule ($D_1^1(2)$, 2.899(4) Å and 173(2)°) (Figure 6 (a)). In this case, the water molecule is placed at an optimal position (even for a contour level as high as 30). The second structure is **CFZ-NH$^+$-CIT$^-$ (1:1)** in which N2 interacts through H-bond with one carboxylic group of dihydrogen citrate ion ($D_1^1(2)$, 2.898(4) Å and 161.6°, Figure 6 (b)). In this structure, the OH from the carboxylic acid interacting with N2 is, however, less optimally placed. While H-bonds between N2 from CFZ and OH from 2,4-DHBA or MeOH could have been expected, such interaction is not observed in the structure of **CFZ-NH$^+$-2,4DHBA$^-$-MeOH (1:1:1)**.

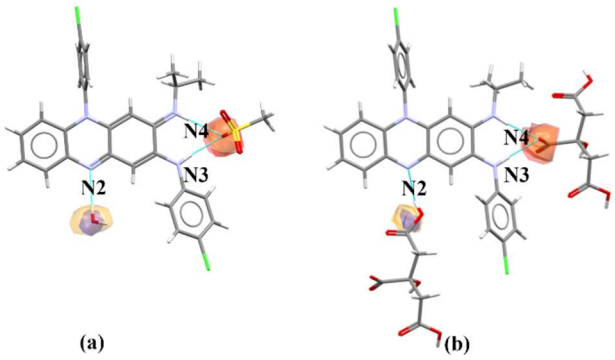

Figure 6 FIMs calculated around clofaziminium from **CFZ-NH$^+$-MSA$^-$-H$_2$O (1:1:1)** (a) and CFZ-NH$^+$ of **CFZ-NH$^+$-CIT$^-$ (1:1)** (b) carbonyl oxygen, uncharged NH and alcohol OH probes in red, blue and orange respectively.

Concerning clofaziminium salts obtained with aliphatic dicarboxylic acids, in currently known structures, proton transfer occurred from one carboxylic acid function, while the other remained protonated. However, in the structures involving the aromatic dicarboxylic acid **CFZ-NH$^+$-TRPTA^{2-}-TRPTA (1:0.5:0.5)** and **CFZ-NH$^+$-TRPTA^{2-}-TRPTA-solvent (1:0.5:0.5:x)**), terephthalate anion is fully unprotonated, leading to three component assemblies (CFZ-NH$^+$-TRPTA^{2-}-CFZ-NH$^+$) bridged together by the remaining terephthalic acid molecule (CFZ and TRPTA were ball milled in 1/1 molar ratio). Double deprotonation of terephthalic acid could eventually be explained by the two low pKa values for this compound (3.54 and 4.34). But interestingly, fumaric acid, which has second pKa value similar to the one of terephthalic acid (pKa of 3.02 and 4.38 for FA) is unprotonated at only one site, forming thus hydrogen fumarate salt of clofazimine. This observation could be explained by the longer distance between carboxylates in TRPTA in comparison with the COOH-COOH distance in

FA (5.803(3) in the structure of **CFZ-NH$^+$-TRPTA^{2-}-TRPTA (1:0.5:0.5)** *vs.* 3.883(3) in the structure of **CFZ-NH$^+$-FA$^-$ (1:1)**).

3.5. Crystal packing comparison

All known clofaziminium salt structures, as well as those described in this paper, were compared by submitting them to the crystal packing similarity tool in CCDC Mercury (Macrae *et al.*, 2008) with a packing shell size of 15 molecules and a distance and angle tolerance of 30% and 30° respectively. Only **CFZ-NH$^+$-SA$^-$ (1:1)** showed a molecular overlay of 15 molecules out of 15 with **CFZ-NH$^+$-MLN$^-$ (1:1)** (GESGOC). This result was quite interesting. Indeed, isostructurality could have been expected between salts implying hydrogen succinate and hydrogen fumarate as counter-ion (as were previously described by J.Galcera et al.) (Galcera & Molins, 2009). However, crystal packing comparison of clofaziminium salts **CFZ-NH$^+$-FA$^-$ (1:1)** and **CFZ-NH$^+$-SA$^-$ (1:1)** indicates a lack of isostructurality. The negative charge on the carboxylate part of hemisuccinate favors the formation of a strong intramolecular H-bond at the expense of intermolecular H-bonds (in contrast to the one observed in **CFZ-NH$^+$-FA$^-$ (1:1)**) preventing isostructurality with **CFZ-NH$^+$-FA$^-$ (1:1)**. This intramolecular H-bond could be similar to the one observed in hydrogen maleate in the structure of **CFZ-NH$^+$-MLE$^-$ (1:1)**, described by G. Bolla and A. Nangia (Bolla & Nangia, 2012). However, no isostructurality is observed with **CFZ-NH$^+$-MLE$^-$ (1:1)**.

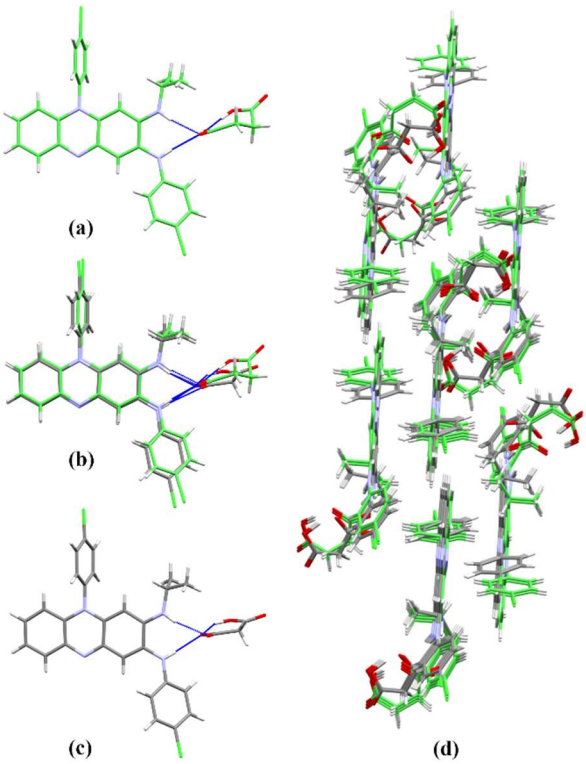

Figure 7 Structure of salt **CFZ-NH$^+$-SA$^-$ (1:1)$_I$** (a), of overlay between **CFZ-NH$^+$-SA$^-$ (1:1)** and **CFZ-NH$^+$-MLN$^-$ (1:1)** (b), and of **CFZ-NH$^+$-MLN$^-$ (1:1)** (c). Crystal packing comparison of **CFZ-NH$^+$-SA$^-$ (1:1)** (green) with **CFZ-NH$^+$-MLN$^-$ (1:1)** salt (grey) (d).

More surprisingly, **CFZ-NH$^+$-SA$^-$ (1:1)** presents isostructurality with **CFZ-NH$^+$-MLN$^-$ (1:1)**, a clofaziminium salt previously described by G. Bolla and A. Nangia (Bolla & Nangia, 2012). The overlay between the crystal lattice of **CFZ-NH$^+$-SA$^-$ (1:1)** and the one of **CFZ-NH$^+$-MLN$^-$ (1:1)** is illustrated in Figure 7. Other crystal packings that are interesting to compare are those of **CFZ-NH$^+$-SACC$^-$—MeCN (1:1:1.4)** and of **CFZ-NH$^+$-TRPTA^{2-}-TRPTA-solvent (1:0.5:0.5:x)** with their non-solvated analogues (**CFZ-NH$^+$-SACC$^-$ (1:1)** and **CFZ-NH$^+$-TRPTA^{2-}-TRPTA (1:0.5:0.5)**). In terms of composition, those salts differ only by the presence or absence of solvent in the structure. However, this solvent may have a strong impact on the crystal packing.Indeed in the non-solvated structure of **CFZ-NH$^+$-SACC$^-$**, a $R_2^1(7)$ H-bond motif is observed between SACC$^-$ and CFZ-NH$^+$ (N4$^+$-H···N5$^-$ and N3-H···N5$^-$) while in the solvated salt a $R_2^2(9)$ motif (N4$^+$-H···O3 and N3-H···N5$^-$) is observed. Such modification of H-bond results in a slight shift in the position of SACC$^-$ (Figure 8). However both structures are quite similar as 14 clofaziminium ions over 15 overlay when solvated and non-solvated structures are analysed by the crystal packing similarity tool in CCDC mercury (Macrae *et al.*, 2008). More structural changes are observed between **CFZ-NH$^+$-TRPTA^{2-}-TRPTA-solvent (1:0.5:0.5:x)** and **CFZ-NH$^+$-TRPTA^{2-}-TRPTA$^-$ (1:0.5:0.5)** (Figure 9 (c)). In the non-solvated structure, H-bonds observed between TRPTA^{2-} and CFZ-NH$^+$ are bifurcated, which is not the case in its solvated analog. Those bifurcated H-bonds lead to major modifications in terms of distance between the planes passing through the main core of CFZ-NH$^+$ (those planes were calculated by taking N1, C5 and C6 atoms of clofaziminium as reference). Indeed, while the inter-plane distance is 6.049Å in the structure of **CFZ-NH$^+$-TRPTA^{2-}-TRPTA-solvent (1:0.5:0.5:x)** (d, Figure 9 (a)), it is only 2.217 Å in the one of **CFZ- NH$^+$-TRPTA^{2-}-TRPTA (1:0.5:0.5)** (d, Figure 9(b)). The differences in crystal packing observed between those two structures result in major changes in terms of (solvent accessible) voids. Indeed in the structure of **CFZ-NH$^+$-TRPTA^{2-}-TRPTA-solvent (1:0.5:0.5:x)**, solvent accessible voids form channels as illustrated at Figure 5 (b) while in that of **CFZ-NH$^+$-TRPTA^{2-}-TRPTA (1:0.5:0.5)** voids are not interconnected and no channel is observed (Figure 5 (d)).

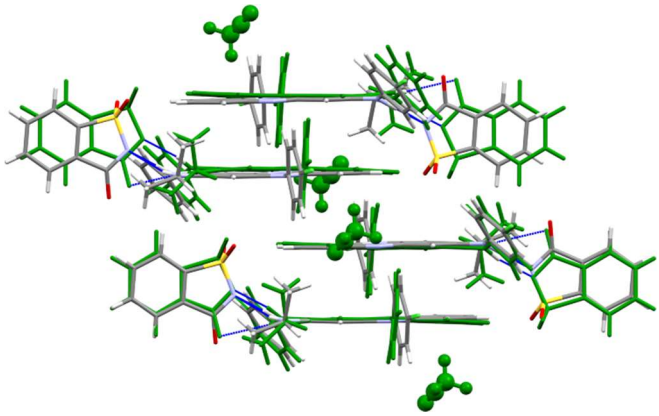

Figure 8 Crystal packing overlay of solvated (green) and non-solvated structures of clofaziminium saccharinate.

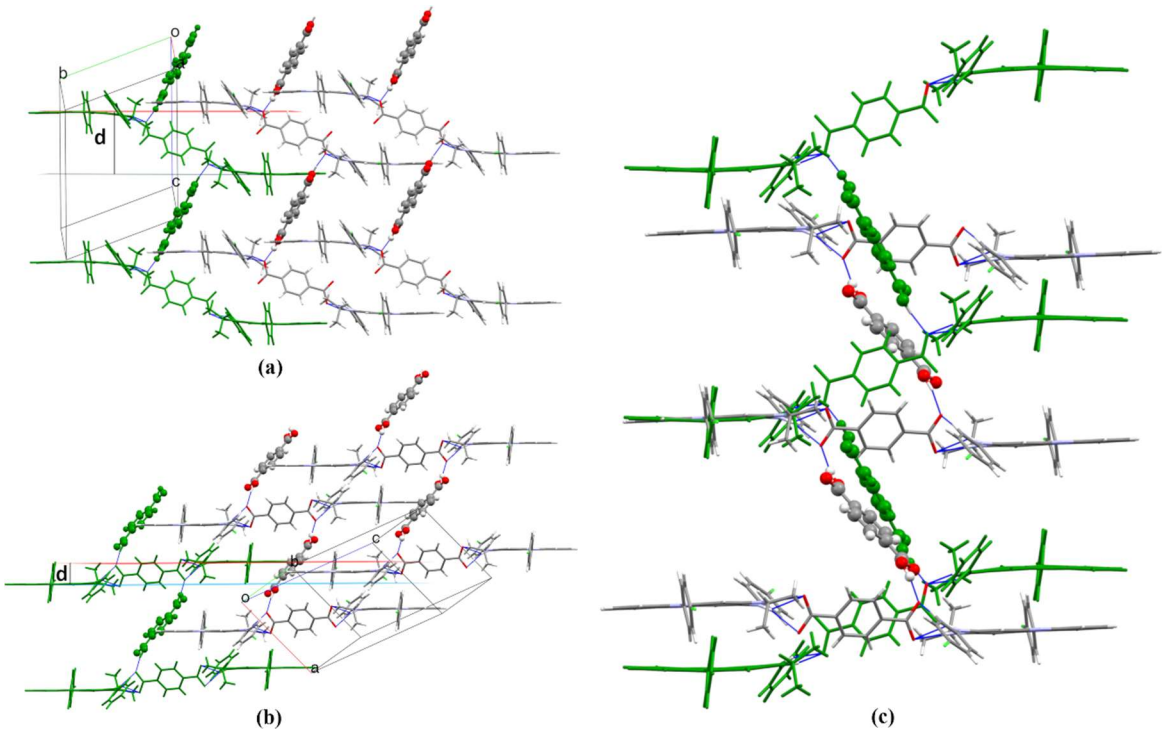

Figure 9 Distance, d, between the planes passing through the main core of **CFZ-NH$^+$** in the structures of **CFZ-NH$^+$-TRPTA^{2-}-TRPTA-solvent (1:0.5:0.5:x)** (a) and **CFZ-NH$^+$-TRPTA^{2-}-TRPTA (1:0.5:0.5)** (b). Crystal packing overlay of solvated (green) and non-solvated structures (c).

3.6. Conformational analysis of clofazimine/clofaziminium.

Clofazimine/clofaziminium conformation is quite restrained, however, conformational changes could be expected around three main torsion angles (T1, T2 and T5 Figure 1) for clofazimine and around four torsion angles for clofaziminium (T1, T2, T4 and T5 Figure 1). T3 torsion angle (Figure 1) is however expected to have values around 90° (because of steric hindrance that would result from T3 torsion angles values different from 90°). To assess the conformational versatility of clofazimine(ium), coordinates were extracted from known structures (from CSD data, and supplementary data from the article of Bannigan *et al.* (Bannigan *et al.*, 2017)) and overlaid (Figure 10 (a) and (b)). Results indicate similar conformations of all clofazimine molecules (Figure 10 (a)) which could be explained by the formation of an intramolecular H-bond between N3-H and N4. Main differences are observed around T1 and T2 torsion angles. T1 and T2 have values around 150 or -150° with two possible combinations: for negative T2 values, T1 can be either positive (CFZ I and II), or negative (Table S3).

Clofaziminium ions also adopt similar conformations (Figure 10 (b)). T1 torsion angle is quite well conserved in salts structures with main values being comprised between 130 and 160°.

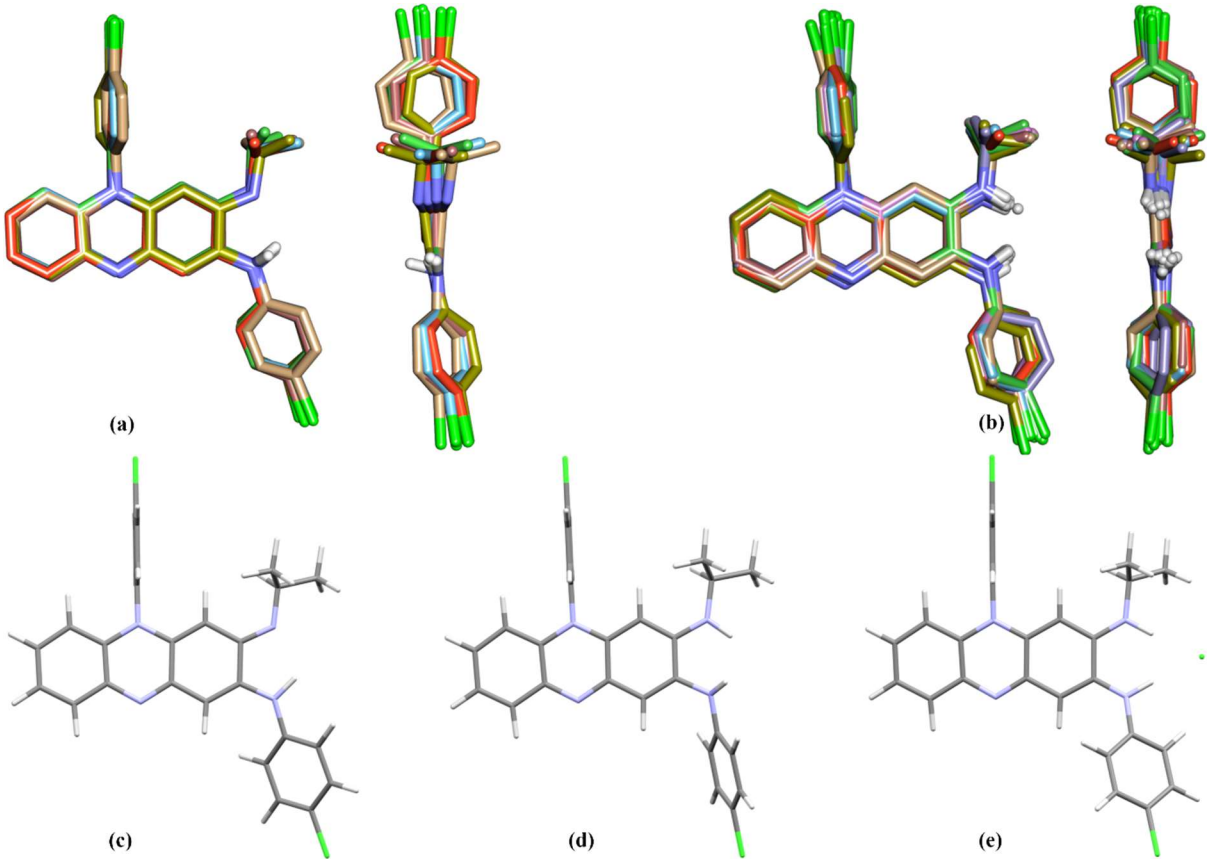

Figure 10 Front and side views after superimposition of clofazimine (a) and clofaziminium (b) conformations, optimized geometries of clofazimine (c), of clofaziminium without any counter-ion (d) and of clofaziminium with Cl^- counter-ion (e).

However, flexibility is observed around T2. Indeed, T2 torsion angle can adopt different values around 150-160°, 90-100°, and 70-80°. More surprising are the values of T4 and T5 torsion angles. Indeed T4 torsion angles are comprised between 0 and 15° while T5 values are mainly comprised between 0 and 20° in absolute value (there are few exceptions: 38° in **CFZ-NH$^+$-SACC$^-$-MeCN (1:1:1.4)**, 31° in **CFZ-NH$^+$-SACC$^-$(1:1)** -28° and 34° in **CFZ-NH$^+$-TRPTA^{2-}-TRPTA-solvent (1:0.5:0.5:x)** and **CFZ-NH$^+$-FA$^-$ (1:1)**). Such values of T4 and T5 result in steric hindrance between the hydrogen atoms positioned on N3 and N4 (distance around those hydrogen atoms is around 1.9 Å (Table S3)). Because of this steric effect, other values of T4 and T5 could be expected, indeed N3-H could be tilted outside the plane of clofazimine. To assess the effect of the counter-ion on CFZ-NH$^+$ conformation, optimization calculations were performed in absence and in presence of the counter-ion (Cl^-), starting from coordinates of clofaziminium chloride (LABQUD) (Figure 9 (d) and (e) and table S5 and S6). Optimization of clofazimine was also performed (starting from coordinates of DAKXUI03) (Figure 10 (c) and Table S4) for the sake of comparison. Optimized CFZ-NH$^+$ conformation confirms the hypothesis of possible higher T5 torsion angle values (T4 = 15.40° and T5= 51.35°). Such a high value of T5 is however never observed in crystal structures. This suggests a quite strong effect of the counter-ion on clofaziminium conformation. Indeed, in clofaziminium salt

crystal structures, the hydrogen atom positioned on N3 remains almost in the plane of clofazimine. This could be explained by the presence of H-bonds between CFZ-NH^+ and its counter-ion, which forces the N3-H to stay close to the clofaziminium plane and compensates for the energy penalty due to steric hindrance. This assumption is supported by the fact that the optimized geometry of CFZ-NH^+ in presence of Cl^- counter-ion results in T5 torsion values much closer, in absolute value, to the ones observed in crystal structures (T4=-3.41° and T5=-11.34° in optimized **CFZ-NH^+-Cl^- (1:1)**) (Figure 10 (e) compared to Figure 10 (b) and Table S3).

4. Conclusions

Six new (solvated/cocrystal of) salts of clofazimine drug with fumaric, succinic, 2,4-dihydroxybenzoic and terephthalic acids as well as with saccharin are reported and compared to the currently known clofaziminium salt structures. While full interaction map analyses reveal two main sites of interaction around clofaziminium, CFZ-NH^+ interaction with its counter-ion mainly occurs at the site located around N3 and N4. Interaction at the second site of clofaziminium is only observed in two structures (**CFZ-NH^+-CIT^- (1:1)** and **CFZ-NH^+-MSA^--H_2O (1:1:1)**) that were already reported. Acid/base reaction between clofazimine and dicarboxylic acids, more often results in single proton transfer (one carboxylic acid function is unprotonated while the other remains protonated) except in the structures implying terephthalic acid (in which COOH-COOH distance is longer than in aliphatic dicarboxylic acids evaluated in the present work). In structures implying terephthalic acid, one terephthalate ion is fully unprotonated while the remaining terephthalic acid molecules serve as bridges between terephthalate anions. Crystal packing comparison of all known structures revealed that **CFZ-NH^+-SA^- (1:1)** and **CFZ-NH^+-MLE^- (1:1)** are isostructural. **CFZ-NH^+-$SACC^-$-MeCN (1:1:1.4)** and **CFZ-NH^+-$TRPTA^{2-}$-TRPTA-solvent (1:0.5:0.5:x)** can be converted to **CFZ-NH^+-$SACC^-$ (1:1)** and **CFZ-NH^+-$TRPTA^{2-}$-TRPTA (1:0.5:0.5)** by solvent evaporation. In both case solvent evaporation leads to structural changes and in H-bond interactions. Crystal packing comparison of those two structures reveals that in clofaziminium saccharinate, anion position is slightly changed while in clofaziminium terephthalate, solvent has a strong impact on H-bond interactions and packing. Indeed, H-bond interactions between CFZ-NH^+ and $TRPTA^{2-}$ change upon drying, leading to the disappearance of solvent accessible channels in favor of isolated voids. In all known structures, clofazimine and clofaziminium adopt similar conformations. The one observed in salt structures may be surprising at first glance because it results in steric hindrance around the protonated site. However conformational optimization of clofaziminium showed the strong impact of the counter-ion on CFZ-NH^+ conformation. Indeed, H-bonds occurring between clofaziminium and the counter-ion compensate the energy penalty due to the steric hindrance. Altogether, these results indicate that despite its quite restrained conformation, clofazimine can crystallize as salts with a high variety of packing, which could lead to different physicochemical and pharmacokinetic properties.

Acknowledgements This work was performed on XRD equipment from the PC2 platform at UNamur. The authors thank CECI platform and Jean Quertinmont for their help with conformational calculations.

Conflicts of interest

The authors declare that the research was conducted in the absence of any commercial or financial relationships that could be construed as a potential conflict of interest.

References

Ash, M. & Ash, I. (2008). Handbook of Food Additives New-York: Synapse Information Resources.

Bannigan, P., Durack, E., Madden, C., Lusi, M. & Hudson, S. P. (2017). *ACS Omega*. **2**, 8969–8981.

Bannigan, P., Zeglinski, J., Lusi, M., O'Brien, J. & Hudson, S. P. (2016). *Cryst. Growth Des.* **16**, 7240–7250.

Barry, V. C., Belton, J. G., Conalty, M. L., Denneny, J. M., Edward, D. W., O'Sullivan, J. F., Twomey, D. & Winder, F. (1957). *Nature*. **179**, 1013–1015.

Basavoju, S., Bostro, D. & Velaga, S. (2008). *Pharm. Res.* **25**, 530–541.

Bolla, G. & Nangia, A. (2012). *Cryst. Growth Des.* **12**, 6250–6259.

Cholo, M. C., Steel, H. C., Fourie, P. B., Germishuizen, W. A. & Anderson, R. (2012). *J. Antimicrob. Chemother.* **67**, 290–298.

Dassault Systèmes BIOVIA (2016).

Dolomanov, O. V., Bourhis, L. J., Gildea, R. J., Howard, J. A. K. & Puschmann, H. (2009). *J. Appl. Crystallogr.* **42**, 339–341.

FDA (2018). SCOGS (Select Committee on GRAS Substances).

Frisch, M. J., Trucks, G. W., Schlegel, H. B., Scuseria, G. E., Robb, M. A., Cheesemen, J. R., Scalmani, G., Barone, V., Petersson, G. A., Nakatsuji, H., Li, X., Caricato, M., Marenich, A. V, Bloino, J., Janesco, B. G., Gomperts, R., Mennucci, B., Hratchian, H. P., Ortiz, J. V, Izmaylov, A. F., Sonnenberg, J. L., Williams-Young, D., Ding, F., Lipparini, F., Egidi, F., Goings, J., Peng, B., Petrone, A., Henderson, T., Ranasinghe, D., Zakrzewski, V. G., Gao, J., Rega, N., Zheng, G., Liang, W., Hada, M., Ehara, M., Toyota, K., Fukuda, R., Hasegawa, J., Ishida, M., Nakajima, T., Honda, Y., Kitao, O., Nakai, H., Vreven, T., Throssell, K., Montgomery, J. A., Peralta, J. J. E., Ogliaro, F., Bearpark, M. J., Heyd, J. J., Brothers, E. N., Kudin, K. N., Staroverov, V. N., Keith, T. A., Kobayashi, R., Normand, J., Raghavachari, K., Rendell, A. P., Burant, J. C., Iyengar, S. S., Tomasi, J., Cossi, M., Millam, J. M., Klene, M., Adamo, C., Cammi, R., Ochterski, J. W., Martin, R. L., Morokuma, K., Farkas, O., Foresman, J. B. & Fox, D. J. (2016). Gaussian 16, Revision A.03 Wallingford CT: Gaussian, Inc.

Frišcic, T., Childs, S. L., Rizvi, S. A. A. & Jones, W. (2009). *CrystEngComm*. **11**, 418–426.

Galcera, J. & Molins, E. (2009). *Cryst. Growth Des.* **9**, 327–334.

Haynes, W. M. Handbook of Chemistry and Physics Boca Raton.

Horstman, E. M., Keswani, R. K., Frey, B. A., Rzeczycki, P. M., LaLone, V., Bertke, J. A., Kenis, P. J. A. & Rosania, G. R. (2017). *Angew. Chemie - Int. Ed.* **56**, 1815–1819.

Hübschle, C. B., Sheldrick, G. M. & Dittrich, B. (2011). *J. Appl. Crystallogr.* **44**, 1281–1284.

James, S. L., Adams, C. J., Bolm, C., Braga, D., Collier, P., Frišcic, T., Grepioni, F., Harris, K. D. M., Hyett, G., Jones, W., Krebs, A., Mack, J., Maini, L., Orpen, A. G., Parkin, I. P., Shearouse, W. C., Steed, J. W. & Waddell, D. C. (2012). *Chem. Soc. Rev.* **41**, 413–447.

Job, C. K., Yoder, L., Jacobson, R. R. & Hastings, R. C. (1990). *J. Am. Acad. Dermatol.* **23**, 236–241.

Keswani, R. K., Baik, J., Yeomans, L., Hitzman, C., Johnson, A. M., Pawate, A. S., Kenis, P. J. A., Rodriguez-Hornedo, N., Stringer, K. A. & Rosania, G. R. (2015). *Mol. Pharm.* **12**, 2528–2536.

Kimyonok, A. B. E. & Ulutürk, M. (2016). *J. Energ. Mater.* **34**, 113–122.

Levy, L. (1974). *Am. J. Trop. Med. Hyg.* **23**, 1097–1109.

Macrae, C. F., Bruno, I. J., Chisholm, J. A., Edgington, P. R., McCabe, P., Pidcock, E., Rodriguez-Monge, L., Taylor, R., Van De Streek, J. & Wood, P. A. (2008). *J. Appl. Crystallogr.* **41**, 466–470.

Narang, A. S. & Srivastava, A. K. (2002). *Drug Dev. Ind. Pharm.* **28**, 1001–1013.

O'Reilly, J. R., Corrigan, O. I. & O'Driscoll, C. M. (1994). *Int. J. Pharm.* **105**, 137–146.

Redd, V. M., O'Sullivan, J. F. & Gangadharam, P. R. J. (1999). *J. Antimicrob. Chemother.* **43**, 615–623.

Rigaku Oxford Diffraction (2015). *CrysAlis PRO*. Rigaku Oxford Diffraction Ltd, Yarnton, England.

Rigaku Oxford Diffraction (2018). *CrysAlis PRO*. Rigaku Oxford Diffraction Ltd, Yarnton, England.

Rowe, R. C., Sheskey, P. J. & Owen, S. C. (2006). Handbook of Pharmaceutical Excipients Pharmaceutical Press and American Pharmacists Association.

Salem, I. I., Steffan, G. & Düzgünes, N. (2003). *Int. J. Pharm.* **260**, 105–114.

Shan, N., Toda, F. & Jones, W. (2002). *Chem. Commun.* **2**, 2372–2373.

Sheldrick, G. M. (2015*a*). *Acta Crystallogr. Sect. C Struct. Chem.* **71**, 3–8.

Sheldrick, G. M. (2015*b*). *Acta Crystallogr. Sect. A Found. Crystallogr.* **71**, 3–8.

Spek, A. L. (2015). *Acta Crystallogr. Sect. C Struct. Chem.* **71**, 9–18.

Temesvári, I., Liptay, G. & Pungor, E. (1971). *E. J. Therm. Anal.* **3**, 293.

Trask, A. V, Motherwell, W. D. S. & Jones, W. (2004). *Chem. Commun.* 890–891.

World Health Organization (2015). Treatment of Tuberculosis.

Zhao, Y. & Truhlar, D. G. (2008). *Theor. Chem. Acc.* **120**, 215–241.

List of Figure and Table captions:

Figure 1: (a) Numbering scheme of clofazimine/ium(CFZ/CFZ-NH^+) (torsions angles: **T1**, C8-N3-C19-C20; **T2**, C9-N4-C25-C27; **T3**, C12-N1-C13-C18 **T4**, H-N4-C9-C8 and **T5**, H-N3-C8-C9) and

selected acids in the present work : fumaric acid, succinic acid, DL-malic acid, 2,4-dihydroxybenzoic acid, saccharin, L-aspartic acid, terephthalic acid and citric acid. (b) Acids crystallized with clofazimine by G. Bolla *et al.* (Bolla & Nangia, 2012) and (c) acids crystallized with clofazimine by P. Bannigan *et al.* (Bannigan *et al.*, 2017). CFZ-NH^+-CIT^- (1:1) salt was already described by P. Bannigan *et al.* (Bannigan *et al.*, 2017), in the present study salt formation of CFZ/CIT in 2/1 and 3/1 molar ratios was attempted.

Figure 2: FIMs calculated around clofazimine (a) and clofaziminium (b). Carbonyl oxygen, uncharged NH and alcohol OH probes in red, blue and orange respectively.

Figure 3: H-bond interactions in the structures of **CFZ-NH^+-FA^- (1:1)** (a), **CFZ-NH^+-SA^- (1:1)** (b), **CFZ-NH^+-$SACC^-$-MeCN (1:1:1.4)** (c), **CFZ-NH^+-$SACC^-$ (1:1)$^-$** (d) **CFZ-NH^+-2,4DHBA$^-$-MeOH (1:1:1)** (e), **CFZ-NH^+-$TRPTA^{2-}$-TRPTA-solvent (1:0.5:0.5:x)** (f) and **CFZ-NH^+-$TRPTA^{2-}$-TRPTA (1:0.5:0.5)** (g). Ellipsoids are drawn at the 50% probability level.

Figure 4: MeOH molecules serve as bridges between 2,4-$DHBA^-$ in the structure of **CFZ-NH^+-2,4DHBA$^-$-MeOH (1:1:1)**.

Figure 5: Three-component assemblies (capped stick) linked by terephthalic acid (ball and stick) of **CFZ-NH^+-$TRPTA^{2-}$-TRPTA-solvent (1:0.5:0.5:x)** (a) and of **CFZ-NH^+-$TRPTA^{2-}$-TRPTA (1:0.5:0.5)** (c). Voids along b-axis (top) and c-axis (bottom) of **CFZ-NH^+-$TRPTA^{2-}$-TRPTA-solvent (1:0.5:0.5:x)** (b) and of **CFZ-NH^+-$TRPTA^{2-}$-TRPTA (1:0.5:0.5)** (d).

Figure 6: FIMs calculated around clofaziminium from **CFZ-NH^+-MSA^--H_2O (1:1:1)** (a) and CFZ-NH^+ of **CFZ-NH^+-CIT^- (1:1)** (b) carbonyl oxygen, uncharged NH and alcohol OH probes in red, blue and orange respectively.

Figure 7: Structure of salt **CFZ-NH^+-SA^- (1:1)** (a), of overlay between **CFZ-NH^+-SA^- (1:1)** and **CFZ-NH^+-MLN^- (1:1)** (b), and of **CFZ-NH^+-MLN^- (1:1)** (c). Crystal packing comparison of **CFZ-NH^+-SA^- (1:1)** (green) with **CFZ-NH^+-MLN^- (1:1)** salt (grey) (d).

Figure 8: Crystal packing overlay of solvated (green) and non-solvated structures of clofaziminium saccharinate.

Figure 9: Distance, d, between the planes passing through the main core of **CFZ-NH^+** in the structures of **CFZ-NH^+-$TRPTA^{2-}$-TRPTA-solvent (1:0.5:0.5:x)** (a) and **CFZ-NH^+-$TRPTA^{2-}$-TRPTA (1:0.5:0.5)** (b). Crystal packing overlay of solvated (green) and non-solvated structures (c).

Figure 10: Front and side views after superimposition of clofazimine (a) and clofaziminium (b) conformations, optimized geometries of clofazimine (c), of clofaziminium without any counter-ion (d) and of clofaziminium with Cl^- counter-ion (e).

Table 1: Clofazimine salification assays and corresponding results.

Table 2: Melting points of non-solvated clofaziminium salts.

Table 3: Experimental details.

Table S1: Published and new structures implying clofazimine or clofaziminium.

Table S2: Selected hydrogen-bond parameters.

Table S3: **T1**, **T2**, **T3**, **T4**, and **T5** torsions angles, C9-N4-C25 angle, and H-H distance between N3-H and N4-H in clofazimine/clofaziminium in published and new structures as well as in optimized structures. Data from structures presented in this work are written in italic. A, B, C and D annotations indicate different molecules in the asymmetric unit while 1 and 2 superscripts indicate the two positions observed in case of disorder. NA means that hydrogen is not present in cif file.

Table S4: Atomic coordinates of optimized clofazimine (DAKXUI03).

Table S5: Atomic coordinates of optimized geometry of clofaziminium without any counter-ion.

Table S6: Atomic coordinates of optimized geometry of clofaziminium with Cl^- counter-ion (LABQUD).

Figure S1: Powder patterns of (a), from bottom to top, CFZ, FA, CFZ/FA LAG MeCN batch powder and **CFZ-NH$^+$FA$^-$ (1:1)** calculated pattern from SCXRD data, (b) CFZ, SA, CFZ/SA LAG MeCN batch powder and **CFZ-NH$^+$-SA$^-$ (1:1)** calculated pattern from SCXRD data, (c) CFZ, SACC, CFZ/SACC LAG MeCN batch powder and **CFZ-NH$^+$-SACC$^-$ (1:1)** and **CFZ-NH$^+$-SACC$^-$-MeCN (1:1:1.4)** calculated patterns from SCXRD data, (d) CFZ, 2,4-DHBA, CFZ/2,4-DHBA LAG MeOH batch powder and **CFZ-NH$^+$-2,4DHBA$^-$-MeOH (1:1:1)** calculated pattern from SCXRD data

Figure S2: Powder patterns of: (a), CFZ, DL-MAL and CFZ/DL-MAL LAG MeCN batch powder, (b) CFZ, L-ASP, CFZ/L-ASP LAG MeCN batch powder, (c) CFZ, TRPTA, CFZ/TRPTA LAG EtOAc, **CFZ-NH$^+$-TRPTA^{2-}-TRPTA-solvent (1:0.5:0.5:x)** calculated pattern from SCXRD data, CFZ/TRPTA LAG EtOAc batch powder at 25°C after heating to 200°C and **CFZ-NH$^+$-TRPTA^{2-}-TRPTA (1:0.5:0.5)** calculated from SCXRD data, (d) CFZ, CIT, **CFZ-NH$^+$-CIT$^-$ (1:1)** calculated from SCXRD data (Bannigan *et al.*, 2017), CFZ/CIT 2/1 LAG MeOH/MeCN 50/50, CFZ-CIT 2/1 calculated from SCXRD data obtained at 100K (structure intrinsically disordered) and CFZ/CIT 3/1 LAG MeOH/MeCN 50/50. * SCXRD data from cif file available in the publication of Bannigan et al. (Bannigan *et al.*, 2017).

Figure S3: (a)Variable temperature powder X-ray diffraction of CFZ/TRPTA LAG EtOAc batch powder and comparison with calculated pattern of **CFZ-NH$^+$-TRPTA^{2-}-TRPTA (1:0.5:0.5)**. Desolvatation of a solvated crystalline powder occurred to give a non-solvated crystalline powder matching the calculated powder pattern of **CFZ-NH$^+$-TRPTA^{2-}-TRPTA (1:0.5:0.5)**. (b) Zoom on the 5-15° 2θ region, disappearing peak upon heating at 2θ value of 7.7° highlighted by plain line frame, appearing peaks upon heating at 2θ values of 8.8 and 9.2° (dashed frame) as well as 11.5 and 12.0° (dotted frame).

Figure S4: Channel arrangement and solvent accessible voids in the structure of **CFZ-NH$^+$-TRPTA^{2-}-TRPTA-solvent (1:0.5:0.5:x)** (view along a-axis) (a) and in the one of **CFZ-NH$^+$-TRPTA^{2-}-TRPTA (1:0.5:0.5)** (view along a-axis) (b).

Figure S5: Effect of different solvents while grinding (a) CFZ with FA, (b) CFZ with SA, (c) CFZ with SACC.

Figure S6: Effect of different solvents while grinding (a) CFZ with TRPTA, (b) CFZ with CIT in 1/1 molar ratio, (c) CFZ with CIT in 2/1 molar ratio and (d) CFZ with CIT in 3/1 molar ratio.

Figure S7: Hirshfeld surface analysis (red regions highlighting close contacts), 2D-fingerprint plots (based on the surface generated on the molecules/ions present in the asymmetric unit) and percentage contribution to the Hirshfeld surface area for the different close contacts in the structures of (a) **CFZ-NH$^+$-FA$^-$ (1:1)** (b) **CFZ-NH$^+$-SA$^-$ (1:1)**, (c) **CFZ-NH$^+$-SACC$^-$-MeCN (1:1:1.4)**, (d) **CFZ-NH$^+$-SACC$^-$(1:1)**, (e) **CFZ-NH$^+$-2,4DHBA$^-$-MeOH (1:1:1)** and (f) **CFZ-NH$^+$-TRPTA^{2-}-TRPTA (1:0.5:0.5)**.

References

Ash, M. & Ash, I. (2008). Handbook of Food Additives New-York: Synapse Information Resources.

Bannigan, P., Durack, E., Madden, C., Lusi, M. & Hudson, S. P. (2017). *ACS Omega*. **2**, 8969–8981.

Bannigan, P., Zeglinski, J., Lusi, M., O'Brien, J. & Hudson, S. P. (2016). *Cryst. Growth Des.* **16**, 7240–7250.

Barry, V. C., Belton, J. G., Conalty, M. L., Denneny, J. M., Edward, D. W., O'Sullivan, J. F., Twomey, D. & Winder, F. (1957). *Nature*. **179**, 1013–1015.

Basavoju, S., Bostro, D. & Velaga, S. (2008). *Pharm. Res.* **25**, 530–541.

Bolla, G. & Nangia, A. (2012). *Cryst. Growth Des.* **12**, 6250–6259.

Cholo, M. C., Steel, H. C., Fourie, P. B., Germishuizen, W. A. & Anderson, R. (2012). *J. Antimicrob. Chemother.* **67**, 290–298.

Dassault Systèmes BIOVIA (2016).

Dolomanov, O. V., Bourhis, L. J., Gildea, R. J., Howard, J. A. K. & Puschmann, H. (2009). *J. Appl. Crystallogr.* **42**, 339–341.

FDA (2018). SCOGS (Select Committee on GRAS Substances).

Frisch, M. J., Trucks, G. W., Schlegel, H. B., Scuseria, G. E., Robb, M. A., Cheesemen, J. R., Scalmani, G., Barone, V., Petersson, G. A., Nakatsuji, H., Li, X., Caricato, M., Marenich, A. V, Bloino, J., Janesco, B. G., Gomperts, R., Mennucci, B., Hratchian, H. P., Ortiz, J. V, Izmaylov, A. F., Sonnenberg, J. L., Williams-Young, D., Ding, F., Lipparini, F., Egidi, F., Goings, J., Peng, B., Petrone, A., Henderson, T., Ranasinghe, D., Zakrzewski, V. G., Gao, J., Rega, N., Zheng, G., Liang, W., Hada, M., Ehara, M., Toyota, K., Fukuda, R., Hasegawa, J., Ishida, M., Nakajima, T., Honda, Y., Kitao, O., Nakai, H., Vreven, T., Throssell, K., Montgomery, J. A., Peralta, J. J. E., Ogliaro, F., Bearpark, M. J., Heyd, J. J., Brothers, E. N., Kudin, K. N., Staroverov, V. N., Keith, T. A., Kobayashi, R., Normand, J., Raghavachari, K., Rendell, A. P., Burant, J. C., Iyengar, S. S., Tomasi, J., Cossi, M., Millam, J. M., Klene, M., Adamo, C., Cammi, R., Ochterski, J. W., Martin, R. L., Morokuma, K., Farkas, O., Foresman, J. B. & Fox, D. J. (2016). Gaussian 16, Revision A.03 Wallingford CT: Gaussian, Inc.

Frišcic, T., Childs, S. L., Rizvi, S. A. A. & Jones, W. (2009). *CrystEngComm*. **11**, 418–426.

Galcera, J. & Molins, E. (2009). *Cryst. Growth Des.* **9**, 327–334.

Haynes, W. M. Handbook of Chemistry and Physics Boca Raton.

Horstman, E. M., Keswani, R. K., Frey, B. A., Rzeczycki, P. M., LaLone, V., Bertke, J. A., Kenis, P. J. A. & Rosania, G. R. (2017). *Angew. Chemie - Int. Ed.* **56**, 1815–1819.

Hübschle, C. B., Sheldrick, G. M. & Dittrich, B. (2011). *J. Appl. Crystallogr.* **44**, 1281–1284.

James, S. L., Adams, C. J., Bolm, C., Braga, D., Collier, P., Frišcic, T., Grepioni, F., Harris, K. D. M., Hyett, G., Jones, W., Krebs, A., Mack, J., Maini, L., Orpen, A. G., Parkin, I. P., Shearouse, W. C., Steed, J. W. & Waddell, D. C. (2012). *Chem. Soc. Rev.* **41**, 413–447.

Job, C. K., Yoder, L., Jacobson, R. R. & Hastings, R. C. (1990). *J. Am. Acad. Dermatol.* **23**, 236–241.

Keswani, R. K., Baik, J., Yeomans, L., Hitzman, C., Johnson, A. M., Pawate, A. S., Kenis, P. J. A., Rodriguez-Hornedo, N., Stringer, K. A. & Rosania, G. R. (2015). *Mol. Pharm.* **12**, 2528–2536.

Kimyonok, A. B. E. & Ulutürk, M. (2016). *J. Energ. Mater.* **34**, 113–122.

Levy, L. (1974). *Am. J. Trop. Med. Hyg.* **23**, 1097–1109.

Macrae, C. F., Bruno, I. J., Chisholm, J. A., Edgington, P. R., McCabe, P., Pidcock, E., Rodriguez-Monge, L., Taylor, R., Van De Streek, J. & Wood, P. A. (2008). *J. Appl. Crystallogr.* **41**, 466–470.

Narang, A. S. & Srivastava, A. K. (2002). *Drug Dev. Ind. Pharm.* **28**, 1001–1013.

O'Reilly, J. R., Corrigan, O. I. & O'Driscoll, C. M. (1994). *Int. J. Pharm.* **105**, 137–146.

Redd, V. M., O'Sullivan, J. F. & Gangadharam, P. R. J. (1999). *J. Antimicrob. Chemother.* **43**, 615–623.

Rigaku Oxford Diffraction (2015). *CrysAlis PRO*. Rigaku Oxford Diffraction Ltd, Yarnton, England.

Rigaku Oxford Diffraction (2018). *CrysAlis PRO*. Rigaku Oxford Diffraction Ltd, Yarnton, England.

Rowe, R. C., Sheskey, P. J. & Owen, S. C. (2006). Handbook of Pharmaceutical Excipients Pharmaceutical Press and American Pharmacists Association.

Salem, I. I., Steffan, G. & Düzgünes, N. (2003). *Int. J. Pharm.* **260**, 105–114.

Shan, N., Toda, F. & Jones, W. (2002). *Chem. Commun.* **2**, 2372–2373.

Sheldrick, G. M. (2015*a*). *Acta Crystallogr. Sect. C Struct. Chem.* **71**, 3–8.

Sheldrick, G. M. (2015*b*). *Acta Crystallogr. Sect. A Found. Crystallogr.* **71**, 3–8.

Spek, A. L. (2015). *Acta Crystallogr. Sect. C Struct. Chem.* **71**, 9–18.

Temesvári, I., Liptay, G. & Pungor, E. (1971). *E. J. Therm. Anal.* **3**, 293.

Trask, A. V, Motherwell, W. D. S. & Jones, W. (2004). *Chem. Commun.* 890–891.

World Health Organization (2015). Treatment of Tuberculosis.

Zhao, Y. & Truhlar, D. G. (2008). *Theor. Chem. Acc.* **120**, 215–241.

Supporting information

Table S1 Published and new structures implying clofazimine or clofaziminium.

Structure	Space Group	a, b, c (Å); α, β, γ (°); V (Å³)	Z	CSD refcode	reference
CFZ (I)	$P\bar{1}$	10.507(4), 12.852(12), 9.601(2); 95.95(4), 97.22(1), 69.73(6); 1204.0(13)	2	DAKXUI01	(Bannigan *et al.*, 2016)
CFZ (II)	$P2_1/a$	7.788(14), 22.960(13), 13.362(7); 90, 98.58(12), 90; 2363(5)	4	DAKXUI	(Bannigan *et al.*, 2016)
CFZ (III)	$Pbca$	23.2417(15), 8.1118(5), 25.5891(16); 90, 90, 90; 4824.4(5)	8	DAKXUI03	(Bannigan *et al.*, 2016)
CFZ (IV)	$P2_1/c$	12.9083, 23.3031, 8.3092; 90, 95.1697, 90; 2489.27	4	DAKXUI02	(Bannigan *et al.*, 2016)
CFZ-DMF	$P\bar{1}$	12.435(4), 12.807(5), 10.424(4); 111.74(3), 112.37(3), 90.90(3); 1402.0(10)	2	CEKTER	(Eggleston *et al.*, 1984)
CFZ-$(CH_3)_2CO$ (1:1)	$P\bar{1}$	10.0842(13), 12.0695(16), 12.6613(16); 75.278(2), 66.588(2), 69.051(2); 1309.3(3)	2	GESHIX	(Bolla & Nangia, 2012)
CFZ-NH^+-$H_2PO_4^-$-H_2O (1:1:0.25)	$P\bar{1}$	14.3064 (9), 15.1345 (9), 27.9096 (17); 96.495 (2), 92.025 (2), 110.640 (2); 5600.4(6)	8	-	(Bannigan *et al.*, 2017)
CFZ-NH^+-HSO_4^--MeOH (1:1:1)	$C2/c$	18.9579(11), 15.4754(9), 20.0404(12); 90, 100.360(2), 90; 5783.6(6)	8	-	(Bannigan *et al.*, 2017)
CFZ-NH^+-MSA^--H_2O (1:1:1)	$P\bar{1}$	9.5945(12), 11.0456(12), 14.4628(11); 110.173(9), 95.859(9), 94.929(9); 1419.1(3)	2	GESHET	(Bolla & Nangia, 2012)
CFZ-NH^+-2,4DHBA$^-$-MeOH (1:1:1)	$P\bar{1}$	9.4861(4), 12.5322(5), 15.3641(5); 98.415(3), 103.379(3), 110.450(4); 1612.40(11)	2	/	This work
CFZ-NH^+-$SACC^-$-MeCN (1:1:1.4)	$P\bar{1}$	7.9970(3), 13.5824(3), 16.6638(7); 80.214(3), 80.034(4), 83.036(3); 1748.87(11)	2	/	This work
CFZ-NH^+-$TRPTA^{2-}$-TRPTA-solvent (1:0.5:0.5:x)	$P\bar{1}$	11.7990(4), 12.0736(4), 14.6803(5); 72.472(3), 80.688(3), 72.030(3); 1891.44(12)	2	/	This work
CFZ-NH^+-Cl^--H_2O (1:1:0.13)	$Pbca$	10.2664(4), 19.8275(7), 24.1558(9); 90, 90, 90; 4917.1(3)	8	RAFHUE	(Horstman *et al.*, 2017)
CFZ-NH^+-Cl^- (1:1)	$Pbca$	10.74739(15), 19.1763(4), 24.2362(3); 90, 90, 90; 4994.96(14)	8	LABQUD	(Keswani *et al.*, 2015)
CFZ-NH^+-MSA^- (1:1)	$P2_1/n$	10.0229 (18), 17.772 (3), 15.592 (3); 90, 103.028 (4), 90; 2705.9(8)	4	GESGAO	(Bolla & Nangia, 2012)
CFZ-NH^+-MLE^- (1:1)	$P2_1/n$	11.2549(19), 20.816(3), 12.519(2); 90, 103.413(17), 90; 2853.0(8)	4	GESHAP	(Bolla & Nangia, 2012)
CFZ-NH^+-INA^- (1:1)	$P\bar{1}$	9.8153(9), 12.1738(10), 15.2122(10); 72.455(7), 77.844(7), 66.479(8); 1580.7(2)	2	GESGES	(Bolla & Nangia, 2012)
CFZ-NH^+-NA^- (1:1)	$P\bar{1}$	11.6032(13), 15.361(2), 18.733(3); 111.337(14), 91.280(11), 109.295(11); 2896.5(8)	4	GESGIW	(Bolla & Nangia, 2012)
CFZ-NH^+-MLN^- (1:1)	$P\bar{1}$	9.8401(8), 12.4069(10), 13.0576(10); 74.129(1), 70.300(1), 67.520(1); 1367.50(19)	2	GESGOC	(Bolla & Nangia, 2012)
CFZ-NH^+-SCL^- (1:1)	$P\bar{1}$	10.8702(6), 11.2066(6), 13.8272(8); 82.354(5), 88.960(5), 63.492(6); 1492.31(17)	2	GESGUI	(Bolla & Nangia, 2012)
CFZ-NH^+-CIT^- (1:1)	$P\bar{1}$	14.7409(6), 15.8211(6), 16.2514(7); 71.928(1), 63.041(1), 70.747(2); 3130.6(2)	4	-	(Bannigan *et al.*, 2017)
CFZ-NH^+-$TRPTA^{2-}$-TRPTA (1:0.5:0.5)	$P\bar{1}$	10.4028 (3), 10.8454 (3), 15.4229 (5); 71.183 (3), 73.984 (3), 76.148 (2); 1561.33 (9)	2	/	This work
CFZ-NH^+-$SACC^-$ (1:1)	$P\bar{1}$	8.2115 (7), 13.5327 (12), 14.325 (3); 89.04 (1), 88.864 (10), 83.781 (7)	2	/	This work
CFZ-NH^+-FA^- (1:1)	$P2_1/c$	7.47882(9), 26.0041(3), 14.78241(16); 90, 102.5075(12), 90; 2806.65(6)	4	/	this work

CFZ-NH$^+$-SA$^-$ (1:1)	$P\bar{1}$	10.6455(6), 12.2850(5), 12.8049(8); 90.076 4), 113.218(6), 108.289(4); 1446.18(15)	2	/	this work

Table S2 Selected hydrogen-bond parameters.

D—H···*A*	*D*—H (Å)	H···*A* (Å)	*D*···*A* (Å)	*D*—H···*A* (°)
CFZ-NH$^+$-FA$^-$ (1:1)				
N3—H3···O2	0.83 (3)	2.48 (3)	3.003 (3)	122 (2)
N3—H3···O3$^-$	0.83 (3)	2.26 (3)	3.040 (3)	156 (3)
N4$^+$—H4···O3$^-$	0.84 (3)	2.17 (3)	2.972 (2)	160 (2)
O1—H1A···O3$^-$	0.94 (4)	1.62 (4)	2.550 (2)	176 (3)
CFZ-NH$^+$-SA$^-$ (1:1)				
N4$^+$—H4···O1$^-$	0.85 (3)	1.98 (3)	2.824 (3)	170 (2)
N3—H3···O1$^-$	0.83 (3)	2.11 (2)	2.871 (3)	152 (3)
O4—H4B···O2$^-$	0.94 (3)	1.56 (3)	2.497 (3)	177 (3)
C15—H15···O1$^-$	0.93	2.31	3.233 (3)	174.6
C29B—H29D···Cl2	0.97	2.80	3.416 (14)	122.2
CFZ-NH$^+$-SACC$^-$ (1:1)				
N4$^+$—H4···N5$^-$	0.79 (7)	2.22 (8)	2.99 (2)	163 (8)
N4$^+$—H4···N5A$^-$	0.79 (7)	2.25 (8)	3.04 (2)	174 (8)
N3—H3···N5$^-$	1.05 (7)	1.78 (7)	2.84 (2)	178 (5)
N3—H3···N5A$^-$	1.05 (7)	1.88 (7)	2.92 (2)	165 (5)
C24—H24···O1	0.93	2.48	3.40 (2)	167.9
C26—H26C···O2	0.96	2.55	3.49 (2)	166.1
C26—H26C···O2A	0.96	2.45	3.370 (18)	160.9
CFZ-NH$^+$-SACC$^-$-MeCN (1:1:1.4)				
N3—H3···N5$^-$	0.87(3)	2.03(3)	2.893(3)	170(3)
N4$^+$—H4N···O3	0.85(4)	2.45(4)	3.264(3)	160(3)
C33—H33···O3	0.95	2.45	3.283(3)	146.0
C24—H24···O1	0.95	2.42	3.314(3)	157.3
CFZ-NH$^+$-2,4DHBA$^-$-MeOH (1:1:1)				
N4$^+$—H4N···O1A$^-$	0.853 (19)	2.00 (2)	2.852 (10)	174.9 (17)
N4$^+$—H4N···O1B$^-$	0.853 (19)	2.00 (3)	2.854 (18)	176.2 (18)
N3—H3N···O1A$^-$	0.89 (2)	1.88 (3)	2.743 (13)	164 (2)
N3—H3N···O1B$^-$	0.89 (2)	1.86 (3)	2.73 (2)	169 (2)
O3A—H3OA···O2A$^-$	1.02	1.66	2.556 (15)	144.5
O4A—H4OA···O5A	0.82	2.02	2.786 (10)	155.2
O5A—H5OA···O3A	0.82	2.39	3.192 (12)	166.6
O3B—H3OB···O2B$^-$	1.02	1.42	2.33 (3)	146.4
O4B— H4OB···O5B	0.82	2.10	2.86 (2)	154.5
O5B—H5OB···O4B	0.82	2.17	2.64 (2)	116.1
C14—H14···O1A$^-$	0.93	2.45	3.346 (11)	161.4
C14—H14···O1B$^-$	0.93	2.57	3.467 (19)	162.1
C23—H23···O4A	0.93	2.50	3.207 (8)	132.8
C23—H23···O4B	0.93	2.41	3.204 (16)	143.3
CFZ-NH$^+$-TRPTA^{2-}-TRPTA-solvent (1:0.5:0.5:x)				
N4$^+$—H4···O1$^-$	0.841 (16)	2.071 (16)	2.8985 (13)	167.7 (15)
N3—H3···O1$^-$	0.866 (18)	1.947 (18)	2.7772 (14)	160.1 (16)

O1A—H3B···$O1^-$	0.91 (2)	1.64 (2)	2.5442 (13)	171 (2)
C15—H15···$O2^-$	0.95	2.44	3.3792 (17)	170.8
CFZ-NH^+-$TRPTA^{2-}$-TRPTA (1:0.5:0.5)				
$N4^+$—H4···$O1^-$	0.86 (2)	1.98 (2)	2.8363 (19)	172.9 (18)
N3—H3···$O2^-$	0.85 (2)	2.17 (2)	2.976 (2)	159 (2)
N3—H3···$O1^-$	0.85 (2)	2.30 (2)	2.996 (2)	140 (2)
O1B—H3B···$O2^-$	0.95 (3)	1.66 (3)	2.5936 (19)	170 (3)
C14—H14···$O1^-$	0.93	2.40	3.276 (2)	156.7
C20—H20···$O2^-$	0.93	2.54	3.307 (2)	139.7
C26—H26C···O2B	0.96	2.55	3.502 (3)	171.5

Table S3 **T1**, **T2**, **T3**, **T4**, and **T5** torsions angles, C9-N4-C25 angle, and H-H distance between N3-H and N4-H in clofazimine/clofaziminium in published and new structures as well as in optimized structures. Data from structures presented in this work are written in italic. A, B, C and D annotations indicate different molecules in the asymmetric unit while 1 and 2 superscripts indicate the two positions observed in case of disorder. NA means that hydrogen is not present in cif file.

Structure	**T1** (°) (C8-N3-C19-C20)	**T2** (°) (C9-N4-C25-C27)	**T3** (°) (C12-N1-C13-C18)	**T4** (°) (H-N4-C9-C8)	**T5** (°) (H-N3-C8-C9)	Angle C9-N4-C25 (°)	H-H distance between N3-H and N4-H
CFZ (I)	154.9(7)	-154.8(8)	92.1(8)	/	-9.9	119.2(5)	/
CFZ (II)	149.4(3)	-157.1(3)	82.1(3)	/	-13(2)	120.7(2)	/
CFZ (III)	-163.1(3)	-152.5(2)	87.8(3)	/	9.6(4)	120.4(2)	/
CFZ (IV)	-146.83	-99.94	110.71	/	0.72	120.71	/
CFZ-DMF	-149.90	-138.45	99.44	/	NA	118.18	/
CFZ-$(CH_3)_2CO$ (1:1)	-146.4(2)	-159.5(2)	97.0(2)	/	5.1	119.2(2)	/
CFZ-NH^+-$H_2PO_4^-$-H_2O (1:1:0.25)	A: 133.8(5) B:-133.6(5) C: 135.2(6) D: 130.7(5)	A: -78.2(5) B: -156.3(4) C: -95.9(6) D: -76.3(7)	A: 63.6(5) B: 93.3(5) C: 82.9(7) D: 91.1(7)	A:-14.4 B: -2.1 C: 1.1 D:-11.3	A: 2.4 B: -1.9 C: -2.1 D: 3.9	A: 125.3(3) B: 124.1(4) C: 127.6(5) D: 125.8(4)	A: 1.8565 B: 1.7934 C: 1.7794 D: 1.8702
CFZ-NH^+-HSO_4^--MeOH (1:1:1)	143.4(2)	-78.8(3)	81.1(3)	1.3	-14.2	124.7(2)	1.8226
CFZ-NH^+-MSA^--H_2O (1:1:1)	174.9(2)	-154.3(3)	95.0(3)	-12(2)	-10.(2)	125.2(2)	1.83(4)
CFZ-NH^+-2,4DHBA$^-$-MeOH (1:1:1)	*-142.18(15)*	*-169.69(14)*	*106.25(15)*	*-1(1)*	*13(2)*	*126.25(13)*	*1.83(3)*
CFZ-NH^+-$SACC^-$-MeCN (1:1:1.4)	*-135.7(2)*	*-144.6(7)* [1] *-69.3(14))* [2]	*91(3)* [1] *99(3)* [2]	*-0(3)*	*38(2)*	*122.8(7)*[1] *129.1(8)*[2]	*2.01(4)*
CFZ-NH^+-$SACC^-$ (1:1)	*-137.0 (6)*	*-158.4 (6)*	*89.7 (7)*	*-12(7)*	*31 (4)*	*126.9 (6)*	*1.9 (1)*
CFZ-NH^+-$TRPTA^{2-}$-TRPTA-solvent (1:0.5:0.5:x)	*143.09(13)*	*-150.77(14)*	*83.78(14)*	*-3(1)*	*-28(1)*	*125.53(10)*	*1.91(3)*
CFZ-NH^+-$TRPTA^{2-}$-TRPTA (1:0.5:0.5)	*-148.7(2)*	*-166.14(17)*	*97.32(18)*	*7(2)*	*24(2)*	*124.72(14)*	*1.97(3)*
CFZ-NH^+-Cl^--H_2O (1:1:0.13)	-149.1(2)	-92.2(3) [1] -137(1) [2]	76.0(2)	13(2)	11(2)	125.7(2) [1] 118.2(5) [2]	2.04(3)
CFZ-NH^+-Cl^- (1:1)	145.9(9)	-149(1)	97(1)	-13(5)	-10(10)	123(1)	1.7(2)
CFZ-NH^+-MSA^- (1:1)	146.5(3)	-71.6(4)	85.4(4)	2(2)	-19(2)	125.9(3)	1.83(4)
CFZ-NH^+-MLE^- (1:1)	-147.2(5)	-100.9(6)	92.8(5)	7(4)	25(3)	125.0(4)	1.98(6)
CFZ-NH^+-INA^- (1:1)	-138.5(4)	-168.5(3)	101.2(4)	-6(2)	21(2)	125.6(3)	1.72(4)
CFZ-NH^+-NA^- (1:1)	A: 142.3(4) B: 150.3(4)	A: -75.8(5) B: -71.0(5)	A: 77.1(4) B: 81.4(4)	A:-10.8 B: -6.2	A: -5.5 B: -5	A: 110.5(3) B: 124.3(3)	A: 1.7938 B: 1.7956
CFZ-NH^+-MLN^- (1:1)	-145.9(3)	-158.0(3)	102.1(3)	1(2)	32.86	125.0(2)	1.99(4)
CFZ-NH^+-SCL^- (1:1)	175.5(2)	-153.5(3)	97.9(2)	-8(2)	-3(2)	125.1(2)	1.92(4)
CFZ-NH^+-CIT^- (1:1)	A: 145.9(3) B: -133.7(3	A: -80.1(3) B:-160.6(3)	A: 89.6(3) B:108.1(3)	A: 5.0 B: 7.6	A:-10.0 B: 0.3	A: 125.6(2) B: 110.8(2)	A: 1.8315 B: 1.8583
CFZ-NH^+-FA^- (1:1)	*-124.4(2)*	*-146.0(3)*	*76.1(2)*	*-8(2)*	*34(2)*	*126.02(18)*	*1.96(4)*
CFZ-NH^+-SA^- (1:1)	*153.0(2)*	*-83.6(3)*	*86.3(2)*	*0(2)*	*-16(2)*	*125.5(2)*	*1.88(4)*
CFZ optimized	-151.32	-156.44	91.63	/	5.62	*121.01*	/
CFZ-NH^+ optimized	-122.86	-159.84	94.07	15.40	51.35	*125.71*	*2.106*
CFZ-NH^+-Cl^- (1:1) optimized	147.26	-151.56	94.71	-3.41	-11.34	*125.56*	*1.793*

Table S4 Atomic coordinates of optimized clofazimine (DAKXUI03).

E (RM06): -2180.82541943 Hartree

center number	atomic number	atomic type	X (Å)	Y (Å)	Z (Å)
1	17	0	8.542442	0.704357	0.209214
2	17	0	-6.9481	-2.29036	0.301462
3	7	0	-2.14619	1.164776	-0.00064
4	7	0	0.140856	2.748417	-0.17926
5	7	0	2.923027	-1.14088	-0.07092
6	1	0	2.783777	-2.15045	-0.13693
7	6	0	-2.28458	2.547588	-0.08207
8	7	0	0.835378	-2.65978	-0.00311
9	6	0	-1.1053	3.314653	-0.17091
10	6	0	-3.85825	0.03082	1.308589
11	1	0	-3.3956	0.426814	2.209955
12	6	0	1.547901	0.863029	-0.11714
13	1	0	2.373254	1.560195	-0.21463
14	6	0	-0.7402	-0.79419	0.042316
15	1	0	-1.60785	-1.44215	0.100702
16	6	0	0.561329	-1.40182	0.001783
17	6	0	-4.9809	-0.77869	1.383768
18	1	0	-5.42362	-1.03208	2.34267
19	6	0	0.249921	1.451792	-0.10542
20	6	0	-2.44695	5.326122	-0.25025
21	1	0	-2.51705	6.408721	-0.31543
22	6	0	-3.31285	0.341952	0.072493
23	6	0	-3.53125	3.17529	-0.08004
24	1	0	-4.44065	2.583892	-0.01418
25	6	0	1.735017	-0.48293	-0.05268
26	6	0	6.878357	0.175384	0.133305
27	6	0	4.226038	-0.65292	-0.00281
28	6	0	5.89341	0.914076	0.766634
29	1	0	6.161099	1.809141	1.321564
30	6	0	-1.21549	4.708614	-0.25385
31	1	0	-0.28766	5.271267	-0.32133
32	6	0	-0.90753	0.555862	-0.01269
33	6	0	-5.53832	-1.26958	0.212642
34	6	0	-3.87643	-0.15388	-1.09399
35	1	0	-3.42727	0.09907	-2.05206
36	6	0	-4.9974	-0.96589	-1.0281
37	1	0	-5.45329	-1.36314	-1.93033
38	6	0	-0.2188	-3.65343	0.025556
39	1	0	-1.04819	-3.32944	0.68098
40	6	0	5.238034	-1.38892	-0.62419
41	1	0	4.975503	-2.28888	-1.17732
42	6	0	-3.60499	4.553147	-0.1635
43	1	0	-4.58073	5.032876	-0.16135
44	6	0	4.573377	0.499034	0.704977
45	1	0	3.814891	1.056259	1.245423
46	6	0	6.557893	-0.98367	-0.55595
47	1	0	7.339542	-1.55883	-1.04455
48	6	0	-0.76555	-3.87152	-1.37932
49	1	0	-1.20876	-2.95781	-1.79154
50	1	0	0.045264	-4.18105	-2.04986
51	1	0	-1.531	-4.65621	-1.38624
52	6	0	0.348687	-4.94272	0.588143
53	1	0	1.160856	-5.30783	-0.05236
54	1	0	0.759522	-4.78602	1.590701
55	1	0	-0.4186	-5.7233	0.648061

Table S5 Atomic coordinates of optimized geometry of clofaziminium without any counter-ion. E(RM06): -2181.23130054 Hartree

center number	atomic number	atomic type	X (Å)	Y (Å)	Z (Å)
1	17	0	7.056535	-1.83325	-0.10889
2	17	0	-8.29076	0.831069	-0.25532
3	7	0	1.986052	1.21845	0.016537
4	7	0	-0.41207	2.611798	0.094537
5	7	0	-2.87044	-1.49724	0.280427
6	1	0	-2.8273	-2.2254	0.987232
7	7	0	-0.57662	-2.84764	-0.11481
8	1	0	-1.50507	-3.19261	-0.33617
9	6	0	3.202897	3.331344	0.012594
10	1	0	4.1611	2.821471	-0.00925
11	6	0	3.14538	4.704976	0.027658
12	1	0	4.072743	5.271274	0.015633
13	6	0	1.917066	5.389851	0.05962
14	1	0	1.906057	6.475633	0.069725
15	6	0	0.745516	4.685901	0.080842
16	1	0	-0.22634	5.17041	0.109056
17	6	0	0.759909	3.274028	0.06823
18	6	0	-0.40737	1.298616	0.083144
19	6	0	-1.64479	0.601186	0.163243
20	1	0	-2.54262	1.205452	0.256108
21	6	0	-1.69997	-0.75572	0.171512
22	6	0	-0.46629	-1.51892	0.014856
23	6	0	0.762381	-0.86201	0.002342
24	1	0	1.678887	-1.43236	-0.08841
25	6	0	0.813821	0.524543	0.038123
26	6	0	2.00929	2.598854	0.029963
27	6	0	3.230027	0.488114	-0.01457
28	6	0	3.827216	0.216216	-1.23502
29	1	0	3.366348	0.567761	-2.15574
30	6	0	5.012574	-0.50068	-1.26552
31	1	0	5.502925	-0.72341	-2.20855
32	6	0	5.576774	-0.935	-0.07274
33	6	0	4.976537	-0.65873	1.149448
34	1	0	5.440162	-1.00187	2.06956
35	6	0	3.792289	0.059804	1.17759
36	1	0	3.30424	0.290501	2.122241
37	6	0	-4.1561	-0.90832	0.167068
38	6	0	-4.5193	-0.24492	-1.0016
39	1	0	-3.8097	-0.16646	-1.82247
40	6	0	-5.78504	0.297301	-1.12814
41	1	0	-6.07633	0.81429	-2.03792
42	6	0	-6.69797	0.159085	-0.09073
43	6	0	-6.35278	-0.51263	1.070791
44	1	0	-7.07718	-0.61536	1.873451
45	6	0	-5.07632	-1.03648	1.200261
46	1	0	-4.79583	-1.54926	2.119174
47	6	0	0.536842	-3.78589	-0.29436
48	1	0	1.238437	-3.33726	-1.0157
49	6	0	-0.01156	-5.06698	-0.88611
50	1	0	-0.73028	-5.53593	-0.20219
51	1	0	0.794397	-5.78635	-1.05265
52	1	0	-0.50696	-4.89353	-1.84702
53	6	0	1.247951	-4.03899	1.023846
54	1	0	1.622656	-3.11914	1.485166
55	1	0	2.101326	-4.70757	0.872355
56	1	0	0.567728	-4.51828	1.736968

Table S6 Atomic coordinates of optimized geometry of clofaziminium with Cl^- counter-ion (LABQUD). E(RM06): -2641.64794122 Hartree

center number	atomic number	atomic type	X (Å)	Y (Å)	Z (Å)
1	17	0	-3.27379	-3.89917	-0.38225
2	7	0	0.095202	2.936519	-0.43037
3	6	0	3.757824	3.303799	-0.11117
4	1	0	4.649915	2.701454	0.035816
5	17	0	-8.09389	1.673677	0.586502
6	7	0	2.334504	1.319351	-0.09732
7	6	0	2.713893	5.464003	-0.40772
8	1	0	2.810042	6.543039	-0.49229
9	7	0	-0.533	-2.49977	-0.3261
10	17	0	7.031537	-2.22103	0.588543
11	6	0	1.477936	4.87299	-0.48096
12	1	0	0.566891	5.448656	-0.62117
13	7	0	-2.78412	-0.84749	-0.14344
14	6	0	1.337	3.476707	-0.37178
15	1	0	-2.91335	-1.87072	-0.25096
16	6	0	2.50132	2.695225	-0.19041
17	6	0	1.100736	0.741508	-0.17869
18	6	0	-0.04056	1.634336	-0.32635
19	6	0	0.909135	-0.61941	-0.14209
20	1	0	1.767179	-1.27377	-0.05894
21	6	0	-1.32675	1.055277	-0.34656
22	1	0	-2.15329	1.749207	-0.44986
23	6	0	-1.55473	-0.29498	-0.23405
24	6	0	-0.37642	-1.19263	-0.23385
25	6	0	-4.01235	-0.18451	0.028548
26	6	0	-5.13582	-0.75764	-0.56983
27	1	0	-5.0168	-1.66719	-1.15531
28	6	0	-6.38655	-0.19398	-0.39573
29	1	0	-7.26117	-0.63977	-0.86074
30	6	0	-6.51852	0.947152	0.379402
31	6	0	-4.16833	0.944026	0.832816
32	1	0	-3.31778	1.365247	1.360611
33	6	0	3.48509	0.476738	0.06962
34	6	0	3.867293	0.090829	1.344782
35	1	0	3.300615	0.441189	2.204705
36	6	0	4.962601	-0.74222	1.508536
37	1	0	5.27952	-1.05787	2.498183
38	6	0	5.657784	-1.17419	0.387891
39	6	0	4.181193	0.042924	-1.04758
40	1	0	3.8581	0.357686	-2.03754
41	6	0	-5.41897	1.513459	1.002824
42	1	0	-5.54386	2.391144	1.630882
43	6	0	5.278596	-0.78842	-0.89006
44	1	0	5.839203	-1.14029	-1.75107
45	6	0	0.54871	-3.4903	-0.33039
46	1	0	1.412921	-3.04428	-0.84218
47	6	0	0.917983	-3.84915	1.099768
48	1	0	1.246471	-2.97446	1.673051
49	1	0	1.724537	-4.59028	1.114467
50	1	0	0.048181	-4.28132	1.608237
51	6	0	0.103184	-4.70726	-1.11753
52	1	0	-0.18416	-4.43898	-2.13881
53	1	0	-0.7644	-5.18499	-0.65038
54	1	0	0.921459	-5.43324	-1.16594
55	6	0	3.85547	4.674	-0.21969
56	1	0	4.834138	5.142751	-0.1577
57	1	0	-1.47856	-2.94228	-0.34855

E(RM06): -2641.64794122 Hartree

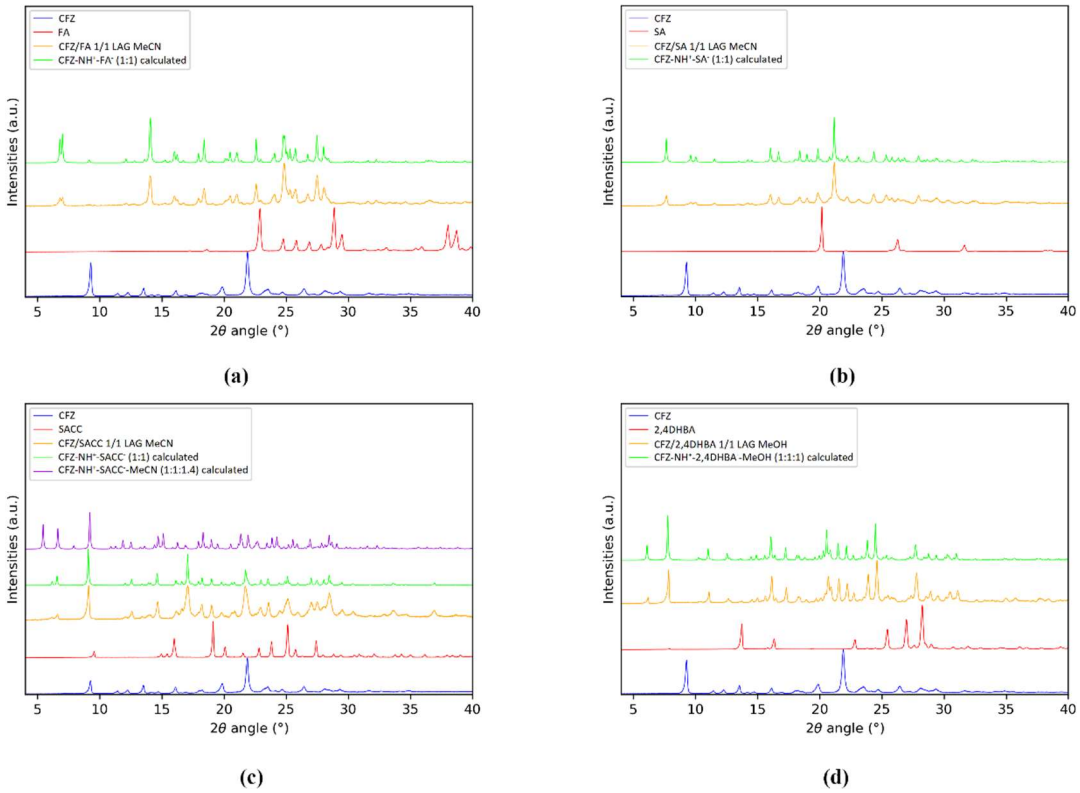

Figure S1 . Powder patterns of (a), from bottom to top, CFZ, FA, CFZ/FA LAG MeCN batch powder and **CFZ-NH$^+$FA$^-$ (1:1)** calculated pattern from SCXRD data, (b) CFZ, SA, CFZ/SA LAG MeCN batch powder and **CFZ-NH$^+$-SA$^-$ (1:1)** calculated pattern from SCXRD data, (c) CFZ, SACC, CFZ/SACC LAG MeCN batch powder and **CFZ-NH$^+$-SACC$^-$ (1:1)** and **CFZ-NH$^+$-SACC$^-$-MeCN (1:1:1.4)** calculated patterns from SCXRD data, (d) CFZ, 2,4-DHBA, CFZ/2,4-DHBA LAG MeOH batch powder and **CFZ-NH$^+$-2,4DHBA$^-$-MeOH (1:1:1)** calculated pattern from SCXRD data.

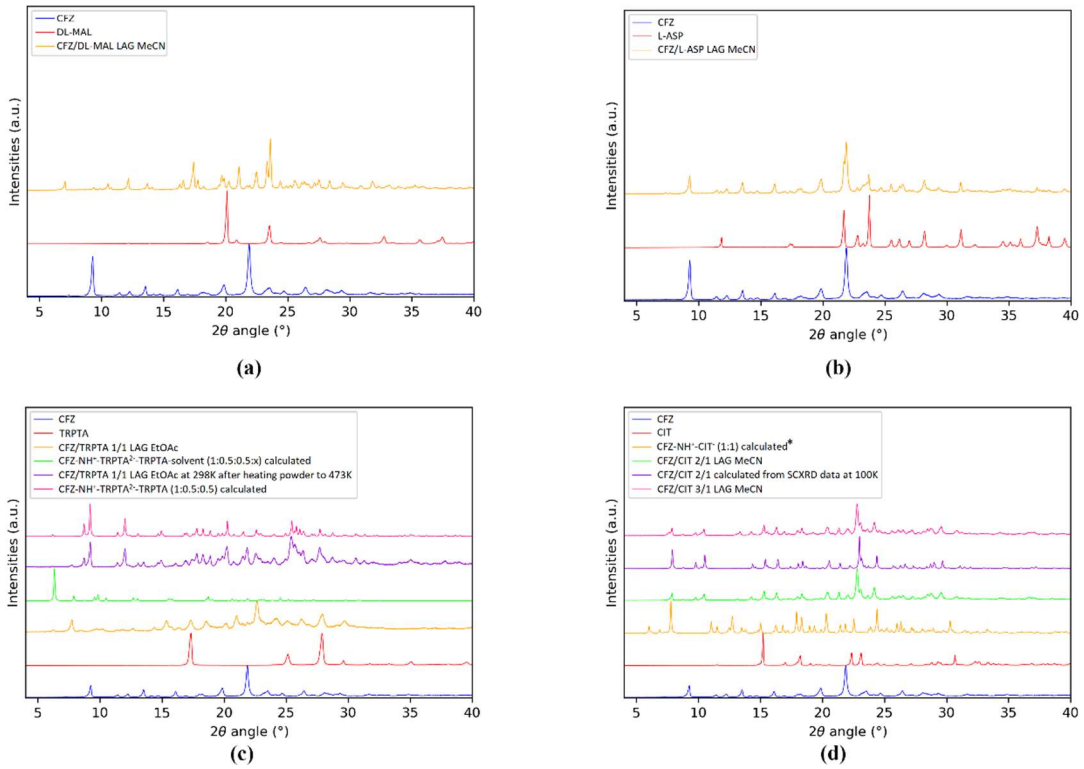

Figure S2 . Powder patterns of (a), CFZ, DL-MAL and CFZ/DL-MAL LAG MeCN batch powder, (b) CFZ, L-ASP, CFZ/L-ASP LAG MeCN batch powder, (c) CFZ, TRPTA, CFZ/TRPTA LAG EtOAc, **CFZ-NH$^+$-TRPTA^{2-}-TRPTA-solvent (1:0.5:0.5:x)** calculated pattern from SCXRD data, CFZ/TRPTA LAG EtOAc batch powder at 25°C after heating to 200°C and **CFZ-NH$^+$-TRPTA^{2-}-TRPTA (1:0.5:0.5)** calculated from SCXRD data, (d) CFZ, CIT, **CFZ-NH$^+$-CIT$^-$ (1:1)** calculated from SCXRD data (Bannigan *et al.*, 2017), CFZ/CIT 2/1 LAG MeOH/MeCN 50/50, CFZ-CIT 2/1 calculated from SCXRD data obtained at 100K (structure intrinsically disordered) and CFZ/CIT 3/1 LAG MeOH/MeCN 50/50. * SCXRD data from cif file available in the publication of Bannigan et al. (Bannigan *et al.*, 2017).

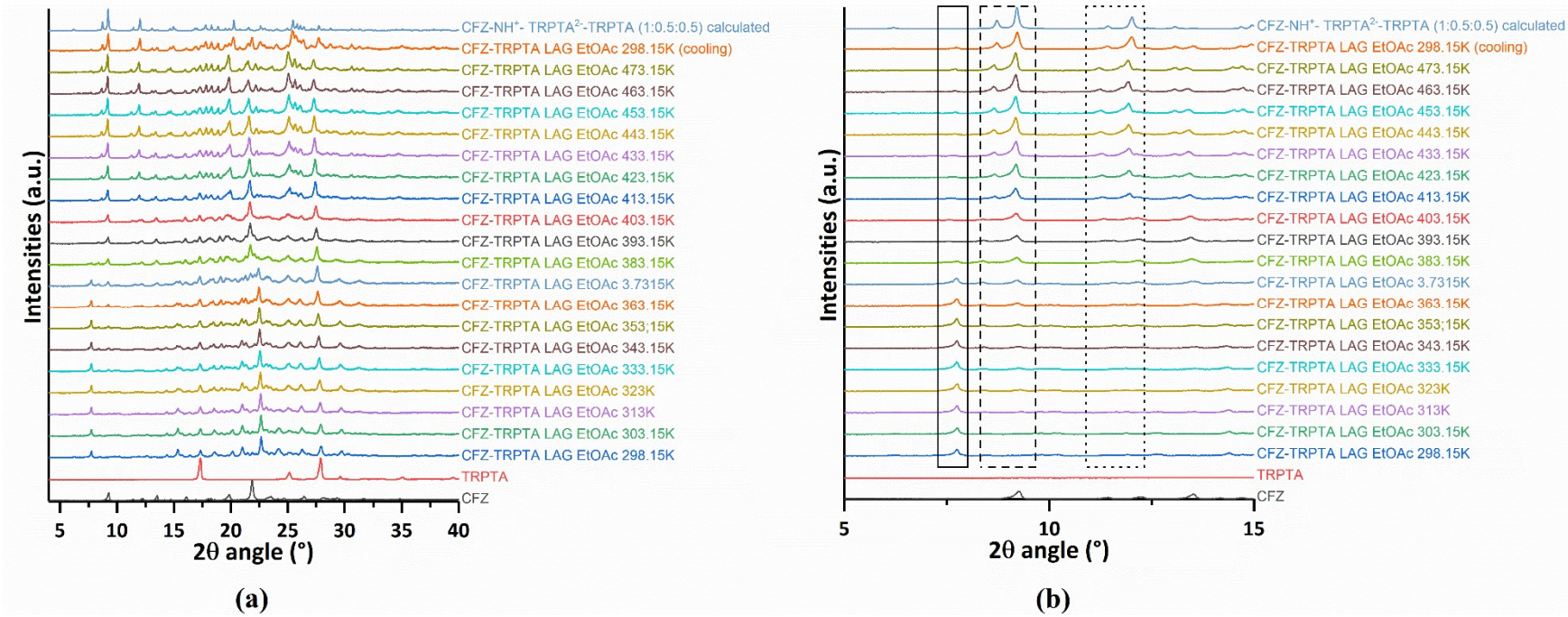

Figure S3 (a)Variable temperature powder X-ray diffraction of CFZ/TRPTA LAG EtOAc batch powder and comparison with calculated pattern of **CFZ-NH$^+$-TRPTA^{2-}-TRPTA (1:0.5:0.5)**. Desolvatation of a solvated crystalline powder occurred to give a non-solvated crystalline powder matching the calculated powder pattern of **CFZ-NH$^+$-TRPTA^{2-}-TRPTA (1:0.5:0.5)**. (b) Zoom on the 5-15° 2θ region, disappearing peak upon heating at 2θ value of 7.7° highlighted by plain line frame, appearing peaks upon heating at 2θ values of 8.8 and 9.2° (dashed frame) as well as 11.5 and 12.0° (dotted frame).

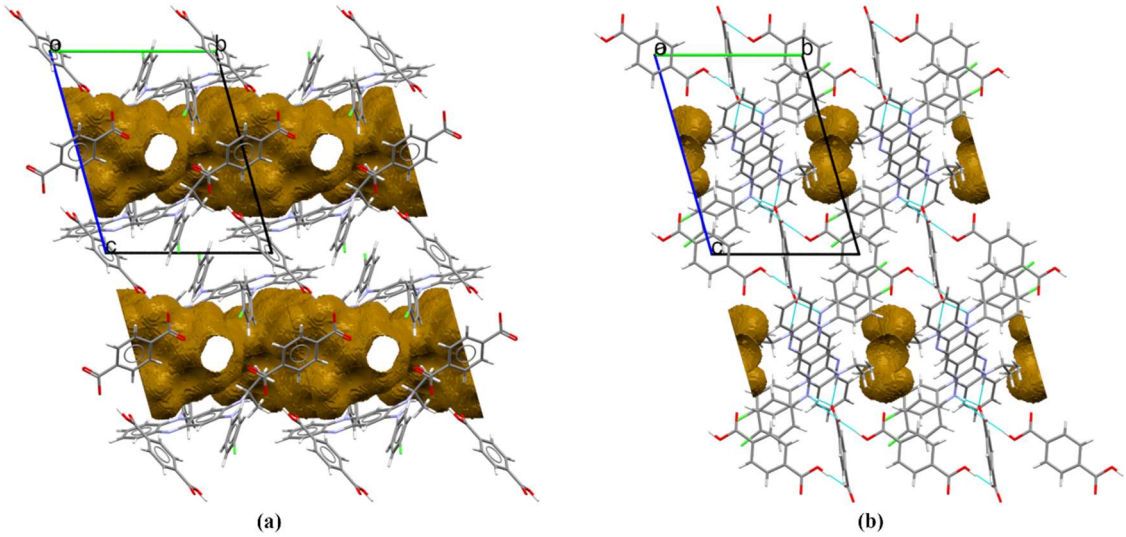

Figure S4 Channel arrangement and solvent accessible voids in the structure of **CFZ-NH$^+$-TRPTA^{2-}-TRPTA-solvent (1:0.5:0.5:x)** (view along a-axis) (a) and in the one of **CFZ-NH$^+$-TRPTA^{2-}-TRPTA (1:0.5:0.5)** (view along a-axis) (b).

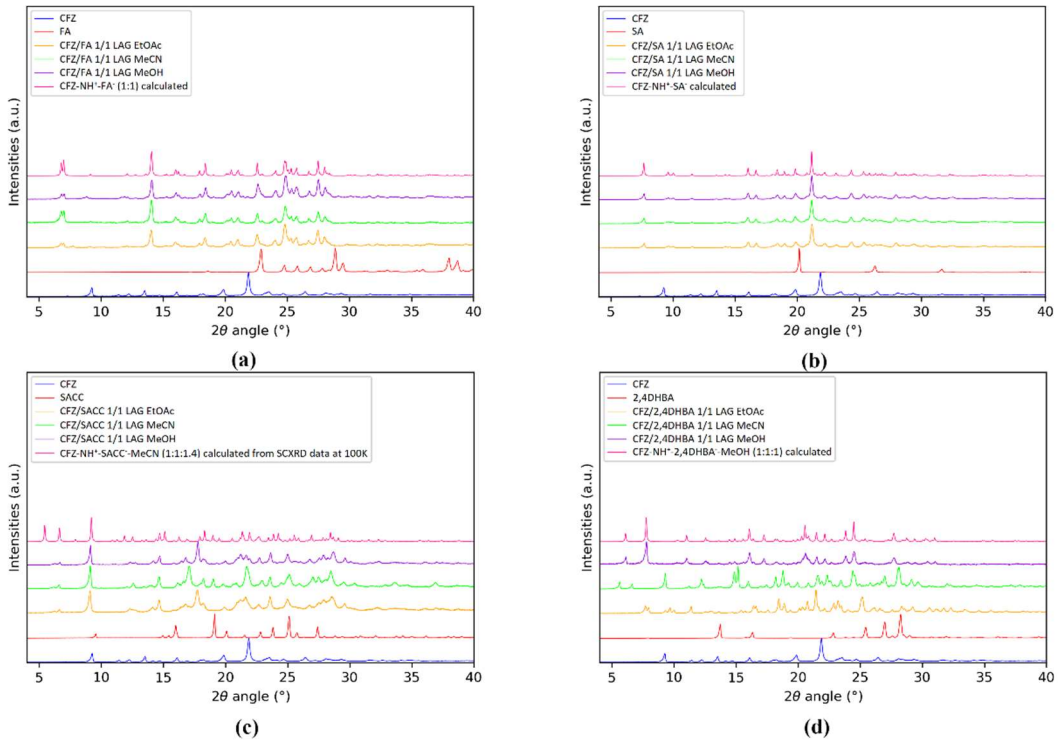

Figure S5 Effect of different solvents while grinding (a) CFZ with FA, (b) CFZ with SA, (c) CFZ with SACC.

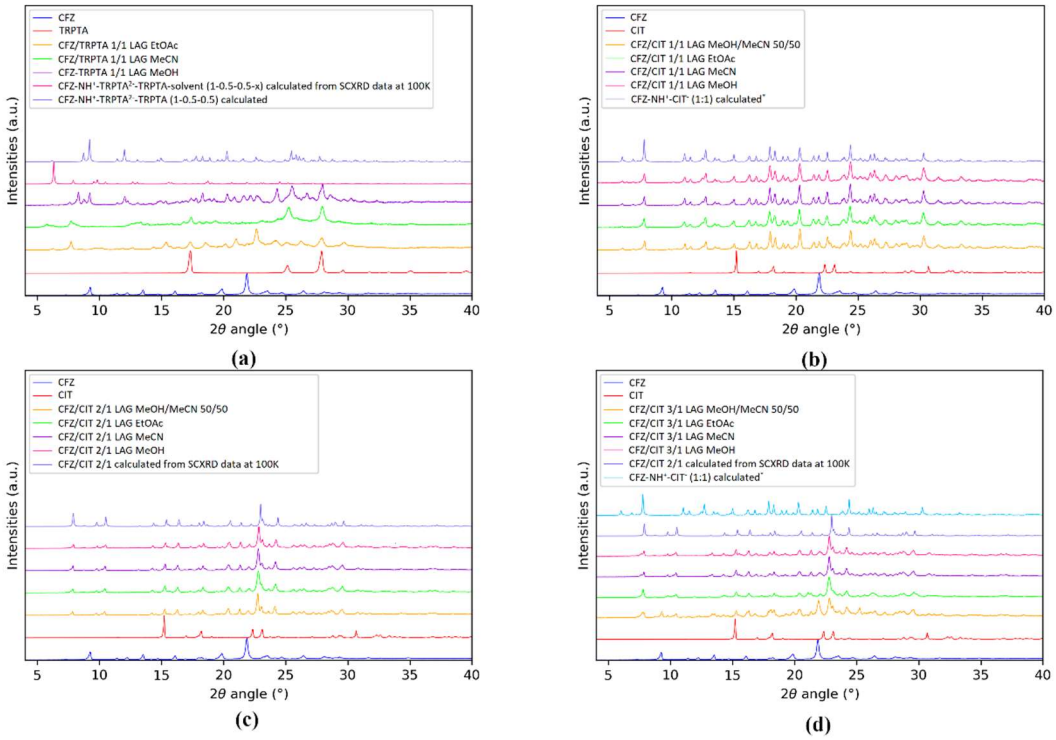

Figure S6 Effect of different solvents while grinding (a) CFZ with TRPTA, (b) CFZ with CIT in 1/1 molar ratio, (c) CFZ with CIT in 2/1 molar ratio and (d) CFZ with CIT in 3/1 molar ratio.

Liquid-assisted grinding experiments were performed in three solvents (MeCN, MeOH and EtOAc) for all combinations described in this paper. For the unsolvated salts, changing the solvent during grinding experiment does not affect the output of the reaction. Instead, for solvated salts, indeed, the powder pattern change in function of the solvent using during liquid-assisted grinding.

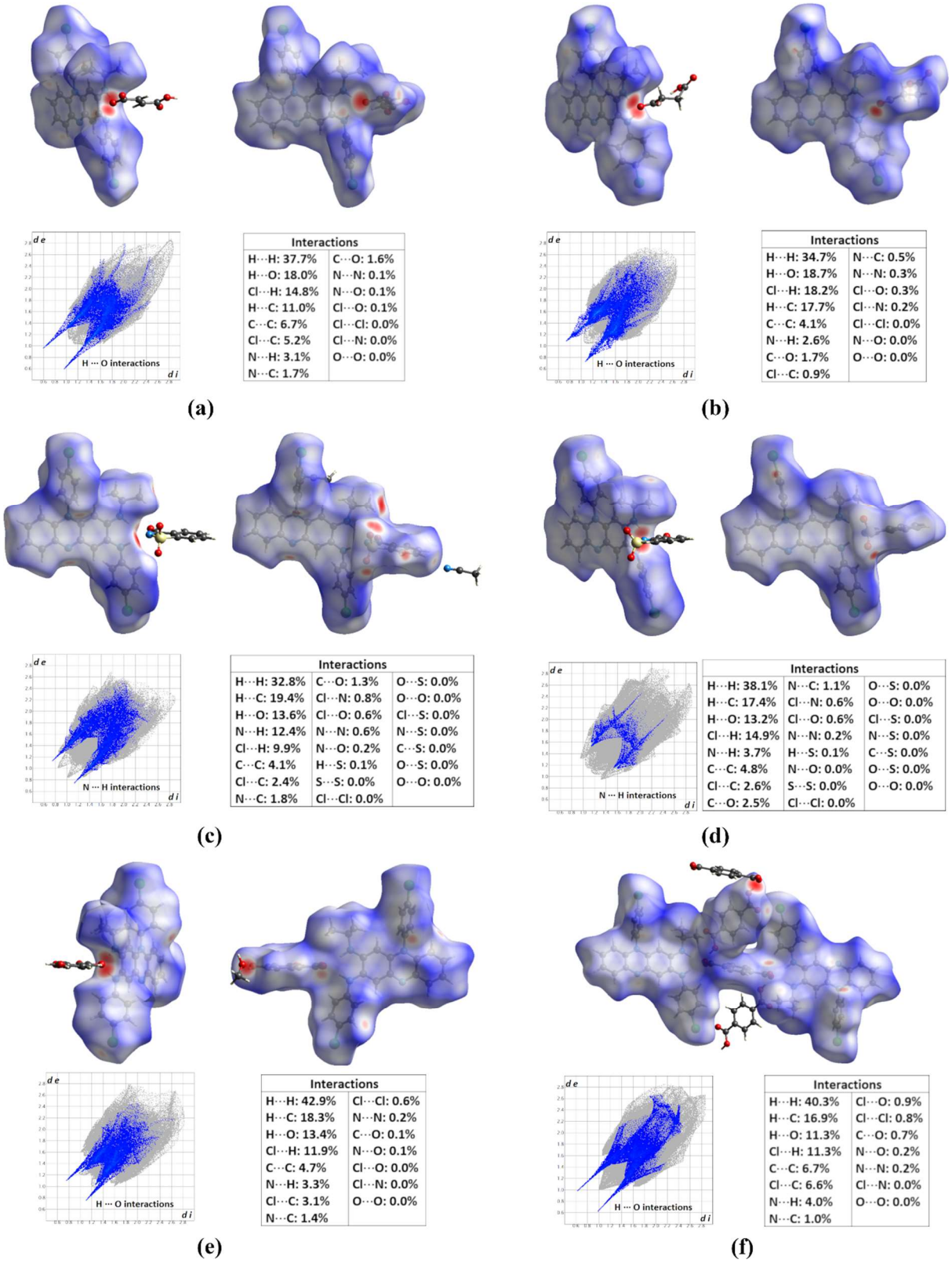

Figure S7 Hirshfeld surface analysis (red regions highlighting close contacts), 2D-fingerprint plots (based on the surface generated on the molecules/ions present in the asymmetric unit) and percentage contribution to the Hirshfeld surface area for the different close contacts in the structures of (a) **CFZ-NH$^+$-FA$^-$ (1:1)** (b) **CFZ-NH$^+$-SA$^-$ (1:1)**, (c) **CFZ-NH$^+$-SACC$^-$-MeCN (1:1:1.4)**, (d) **CFZ-NH$^+$-**

SACC$^-$(1:1), (e) **CFZ-NH$^+$-2,4DHBA$^-$-MeOH (1:1:1)** and (f) **CFZ-NH$^+$-TRPTA^{2-}-TRPTA (1:0.5:0.5)**.

Hirshfeld surfaces and fingerprint plots of d_e (distance from the surface to the nearest atoms outside the surface) *vs.* d_i (distance from the surface to the nearest atoms located inside the surface) were generated using CrystalExplorer (version 17.5) (Turner *et al.*, 2017; Spackman & Jayatilaka, 2009; Spackman & Mckinnon, 2002; Hirshfeld, 1977). Surfaces were generated using the normalized contact distance 'd_{norm}' descriptor (Mckinnon *et al.*, 2007). White surfaces correspond to contacts with distance around the sum of van der Waals radii while red and blue surfaces highlight shorter and longer contacts respectively (Mckinnon *et al.*, 2007). For the structure of **CFZ-NH$^+$-SA$^-$ (1:1)** disorder of SA$^-$ was removed (and occupancies of C29A, H29A, H29B, C30A, H30A and H30B were modified from 0.739 to 1) for surface and fingerprint plots generation. For the structure of **CFZ-NH$^+$2,4DHBA$^-$-MeOH (1:1:1)** 2,4DHBA$^-$ and MeOH disorder was removed and corresponding occupancies were modified to 1. Concerning the structure of **CFZ-NH$^+$-SACC$^-$-MeCN (1:1:1.4)** MeCN is disordered over three position, with positions of C37-C38-N7 being very close to the ones of C37A-C38A-N7A. In consequence, one MeCN molecule (C37A-H37D-H37E-H37F-C38A-N7A) was removed and occupancies of C37-H37A-H37B-H37C-C38-N7 were modified accordingly (occupancies of 0.464 modified to 0.953 (which is the sum of the occupancies of C37A-H37D-H37E-H37F-C38A-N7A and C37-H37A-H37B-H37C-C38-N7). Disorder of isopropyl of CFZ was also removed and occupancies of C25B-H25B-C26B-H26D-H26E-H26F-C27B-H27D-H27E-H27F were modified to 1 before Hirshfeld surface and 2D fingerprint plots generation. In the structure of **CFZ-NH$^+$-SACC$^-$ (1:1:)**, SACC$^-$ is disordered and second position of SACC was removed (and occupancies were modified to 1 for the remaining SACC position) prior Hirshfeld surface and 2D fingerprint plots generation. 2D-fingerprint plots shown on Figure S7 corresponds to the Hirshfeld surface generated by selecting all atoms from the unit cell (for **CFZ-NH$^+$-TRPTA^{2-}-TRPTA (1:0.5:0.5)**, Hirshfeld surface was generated on **CFZ-NH$^+$-TRPTA^{2-}-TRPTA-CFZ-NH$^+$ (1:1:1:1**) assembly which corresponds to a charge balanced assembly).

References

Bannigan, P., Durack, E., Madden, C., Lusi, M. & Hudson, S. P. (2017). *ACS Omega*. **2**, 8969–8981.

Bannigan, P., Zeglinski, J., Lusi, M., O'Brien, J. & Hudson, S. P. (2016). *Cryst. Growth Des.* **16**, 7240–7250.

Bolla, G. & Nangia, A. (2012). *Cryst. Growth Des.* **12**, 6250–6259.

Eggleston, D. S., Marsh, W. E. & Hodgson, D. J. (1984). *Acta Crystallogr.* **C40**, 288–292.

Hirshfeld, F. L. (1977). *Theor. Chim. Acta*. **44**, 129–138.

Horstman, E. M., Keswani, R. K., Frey, B. A., Rzeczycki, P. M., LaLone, V., Bertke, J. A., Kenis, P. J. A. & Rosania, G. R. (2017). *Angew. Chemie - Int. Ed.* **56**, 1815–1819.

Keswani, R. K., Baik, J., Yeomans, L., Hitzman, C., Johnson, A. M., Pawate, A. S., Kenis, P. J. A., Rodriguez-Hornedo, N., Stringer, K. A. & Rosania, G. R. (2015). *Mol. Pharm.* **12**, 2528–2536.

Mckinnon, J. J., Jayatilaka, D. & Spackman, M. A. (2007). *Chem. Commun.* 3814–3816.

Spackman, M. A. & Jayatilaka, D. (2009). *CrystEngComm*. **11**, 19–32.

Spackman, M. A. & Mckinnon, J. J. (2002). *CrystEngComm*. **4**, 378–392.

Turner, M. J., McKinnon, J. J., Wolff, S. K., Grimwood, D. J., Spackman, P. R., Jayatilaka, D. & Spackman, M. A. (2017). University of Western Australia.